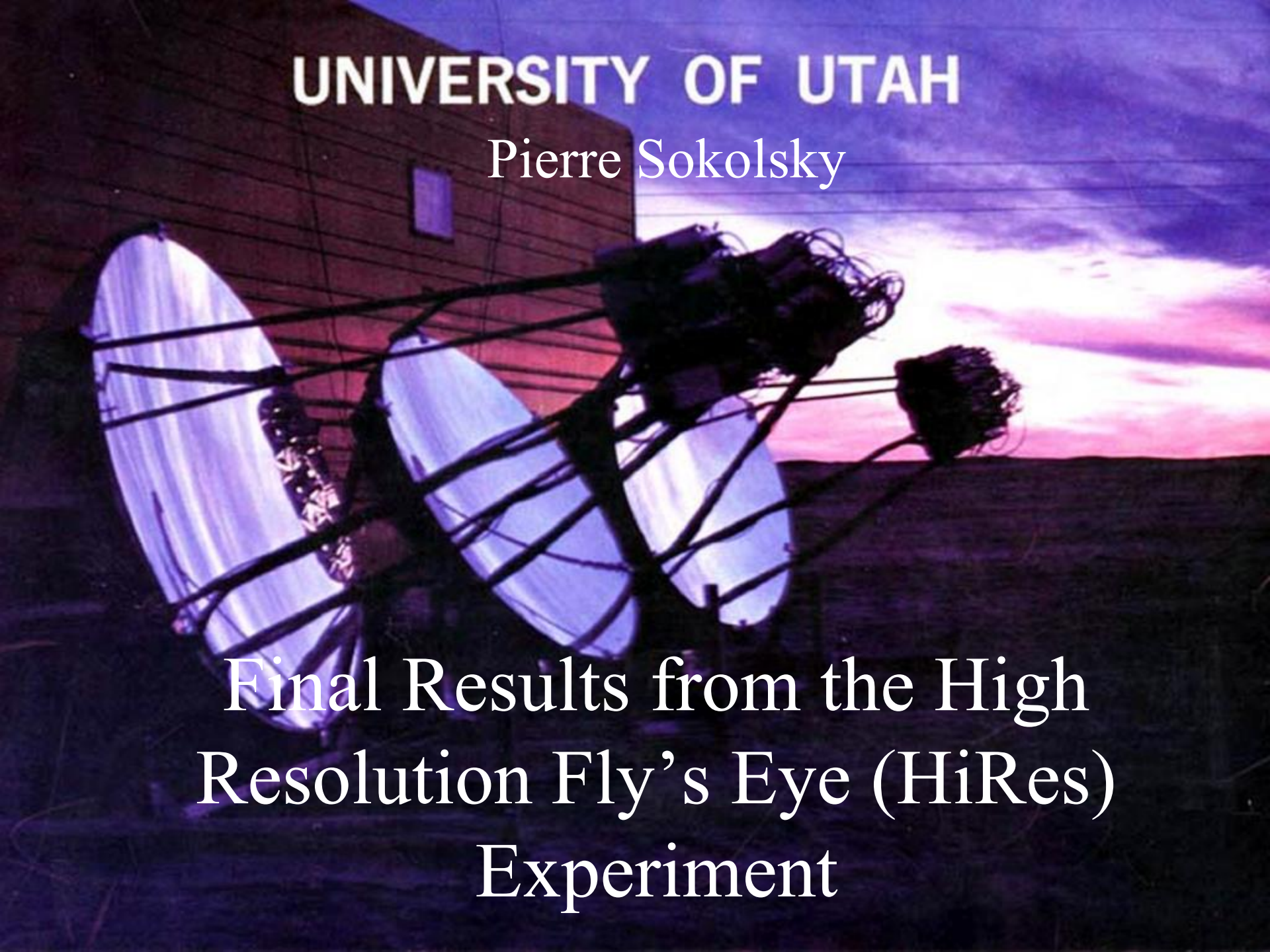

Pierre Sokolsky

Final Results from the High Resolution Fly's Eye (HiRes) Experiment

High Resolution Fly's Eye Collaboration:

S. BenZvi, J. Boyer, B. Connolly, C.B. Finley, B. Knapp, E.J. Mannel, A. O'Neill, M. Seman, S. Westerhoff

Columbia University

J.F.Amman, M.D.Cooper, C.M.Hoffman, M.H. Holzscheiter, C.A.Painter, J.S.Sarracino, G.Sinnis, T.N.Thompson, D.Tupa

Los Alamos National Laboratory

J. Belz, M. Kirn

University of Montana

J.A.J. Matthews, M. Roberts

University of New Mexico

D.R. Bergman, G. Hughes, D. Ivanov, S.R. Schnetzer, L. Scott, S. Stratton, G.B. Thomson, A. Zech

Rutgers University

N. Manago, M. Sasaki

University of Tokyo

R.U.Abbasi, T.Abu-Zayyad, G.Archbold, K.Belov, O.Brusova, S.A..Blake, Z.Cao, W.Deng, R.C.Gray, W.Hanlon, Y.Fedorova, P.Huentemeyer, B.F Jones, C.C.H.Jui, **E.C.Loh**, M.M.Maestas, K.Martens, J.N.Matthews, S.A.Moore, K.Reil, D.Rodriguez,,P.Shen, J.Smith, P.Sokolsky, R.W.Springer, B.T.Stokes, J.R.Thomas, S.B.Thomas, L.Wiencke

University of Utah

Until recently, HiRes was located on the U.S. Army's Dugway Proving Ground, ~100 miles south-west of the University of Utah

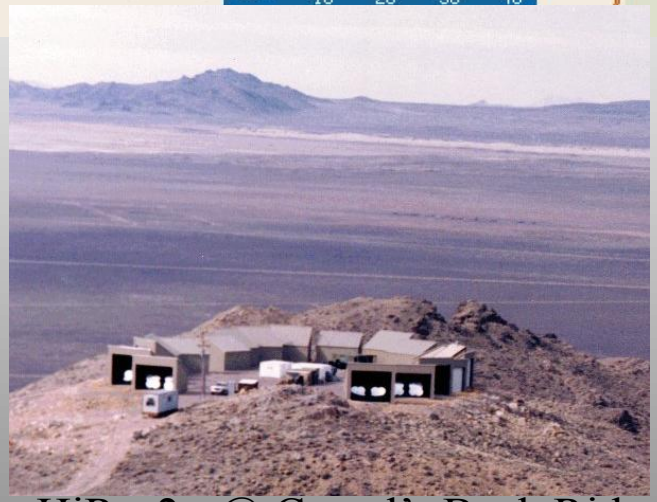

- HiRes1: @ Five Mile Hill (aka Little Granite Mountain)
- 21 mirrors, 1 ring (3^{o}<altitude<17^{o})
- Sample-and-hold electronics (pulse height and trigger time)

- HiRes2: @ Camel's Back Ridge 12.6 km south-west of HiRes1.
- 42 mirrors, 2 rings (3^{o}<altitude<31^{o})
- FADC electronics (100 ns period)

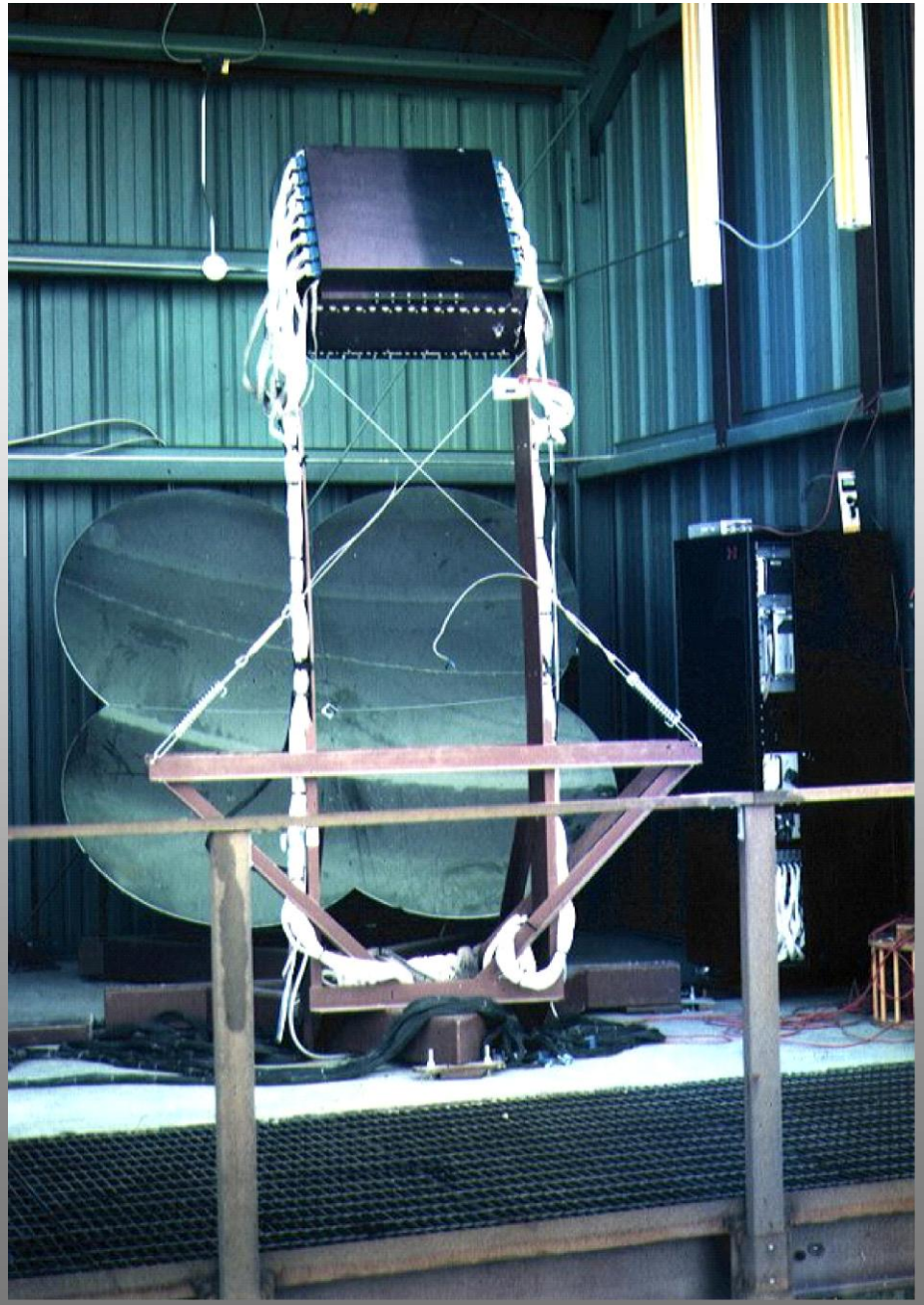

HiRes Spectrum

- Monocular spectra - HiRes I and II
- HiRes I - largest statistics, limited elevation angle viewing = high threshold energy
- HiRes II - best low energy response
- Stereo spectrum - best geometrical and energy resolution

Reconstruction

- The trajectory of the EAS can be determined in one of two ways:
  1. Monocular reconstruction using the arrival time of light signal at the detector.
  2. By intersecting the shower-detector planes (SDP) seen from the two detector sites.

1.)

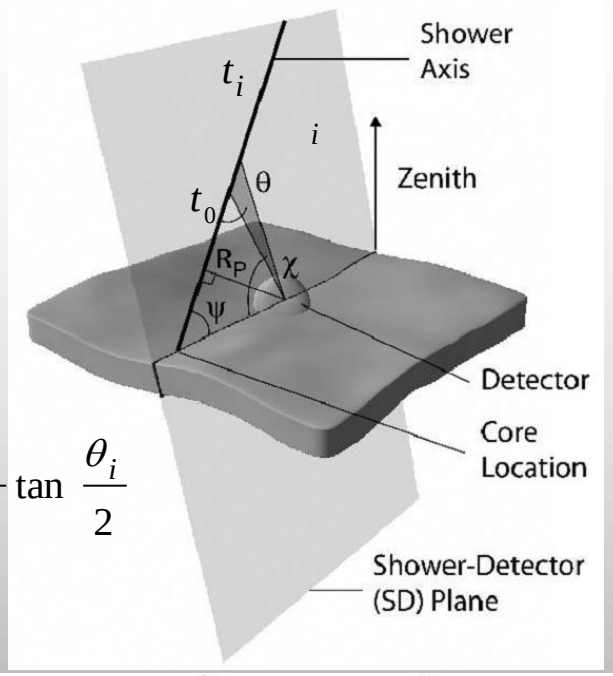

$$t_i = t_0 + \frac{R_P}{c} \tan \frac{\theta_i}{2}$$

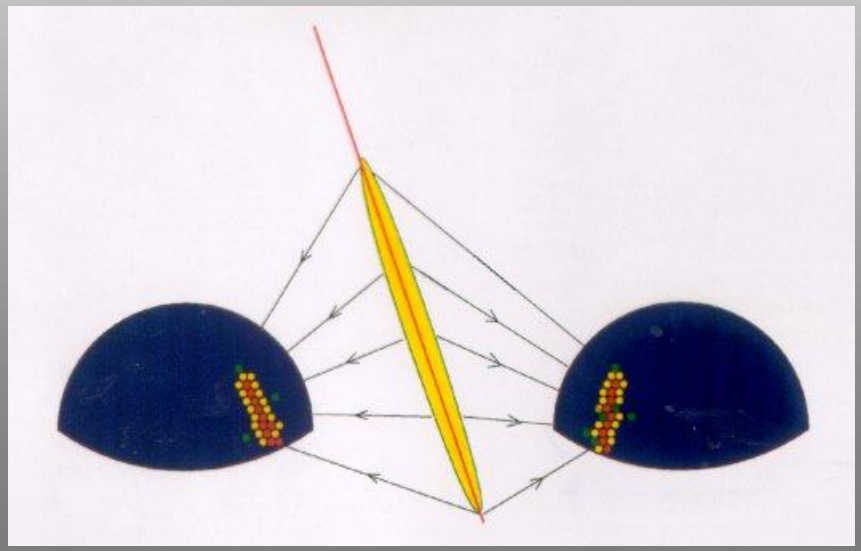

2.)

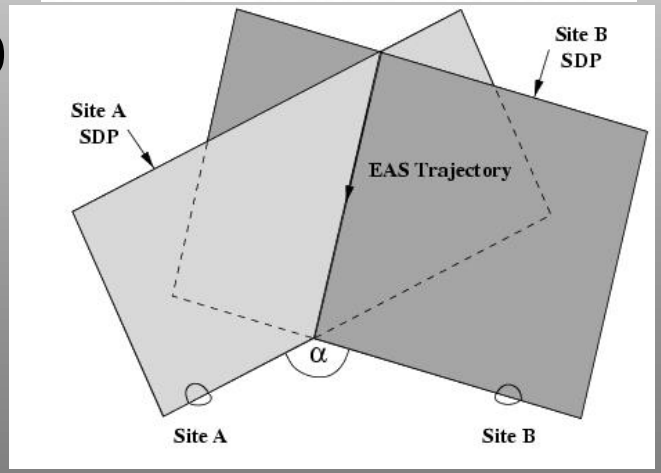

Typical Stereo HiRes Event:

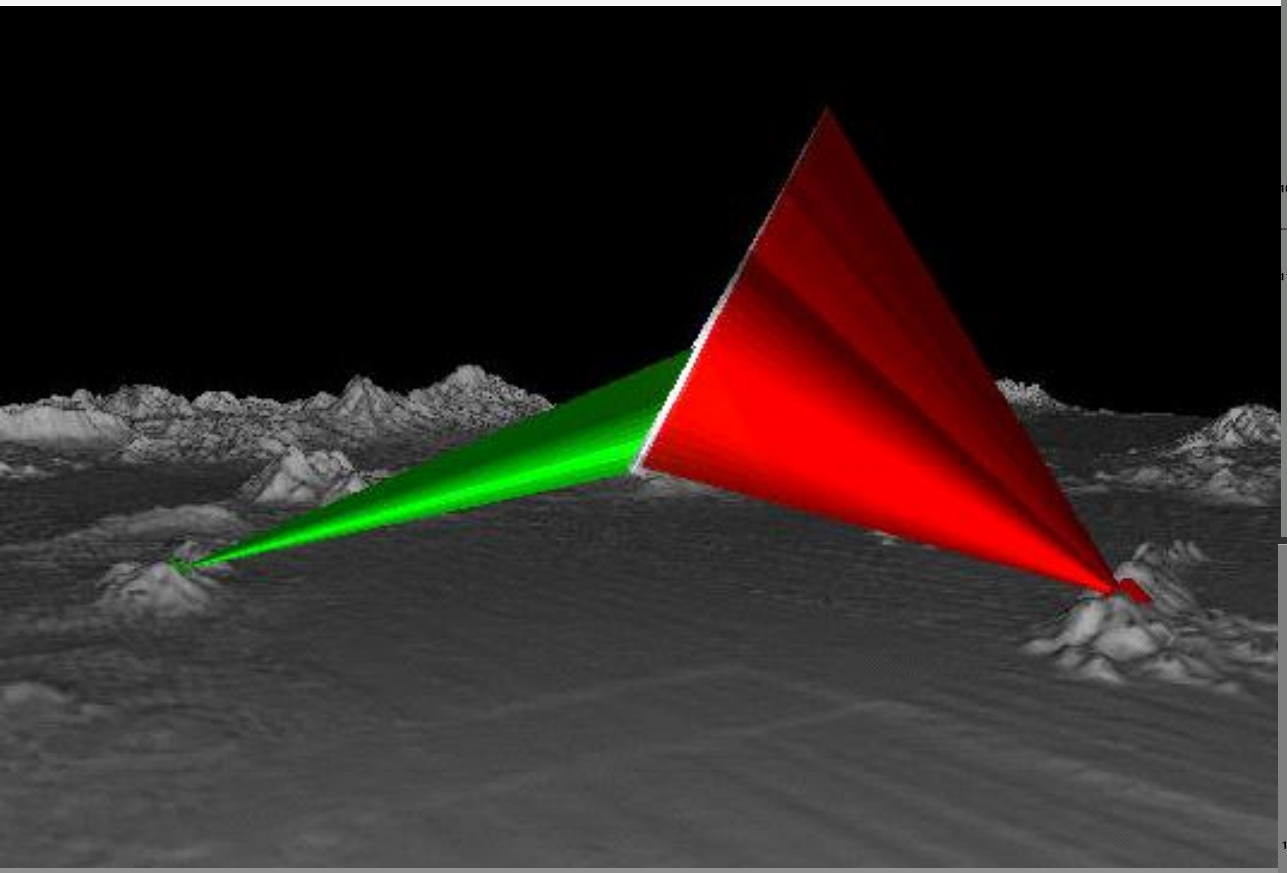

Looking South

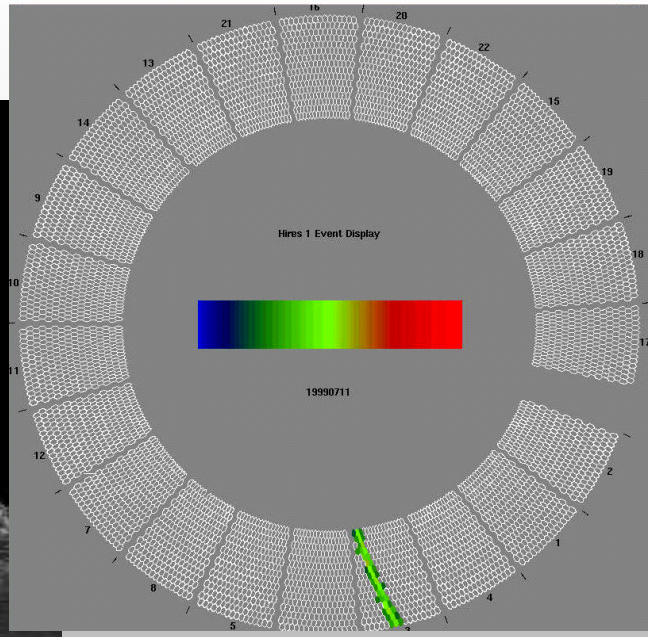

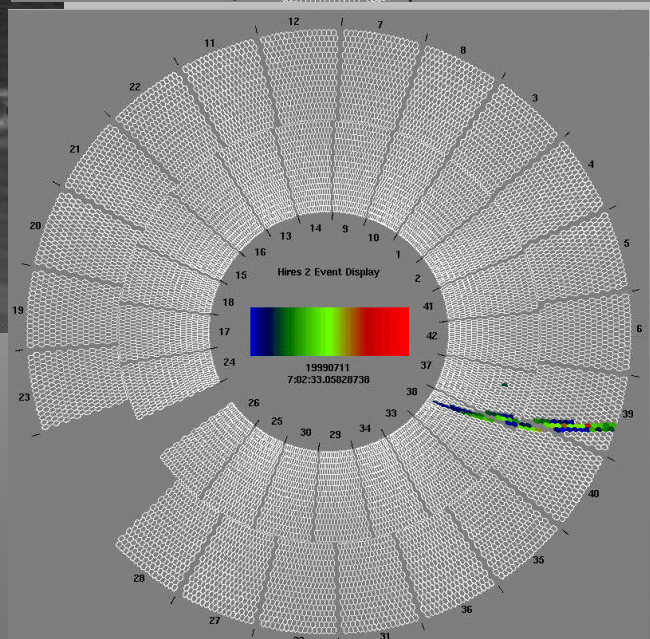

Measured Shower Profile

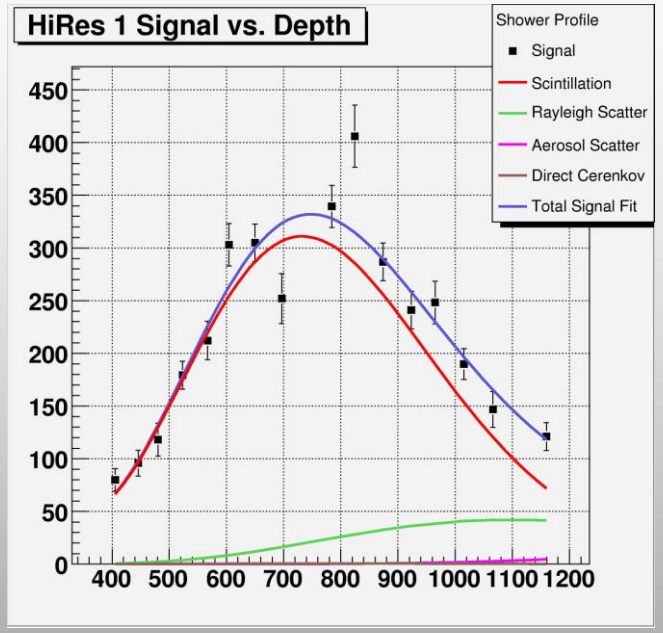

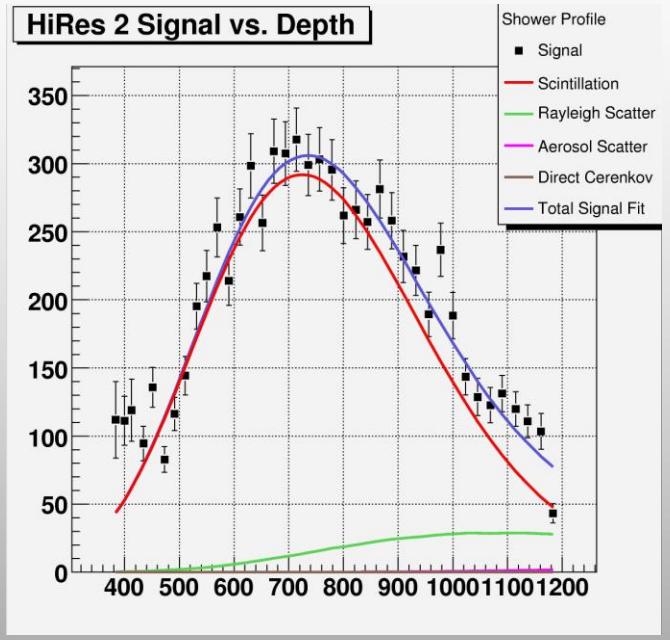

Measured shower parameters.

Event by event:

- X_{max} in g/cm^2;
- Total energy of the primary particle:
- Arrival direction

Statistically:

- Mass composition
- *p*-air inelastic cross-section

Monocular and Stereo Aperture

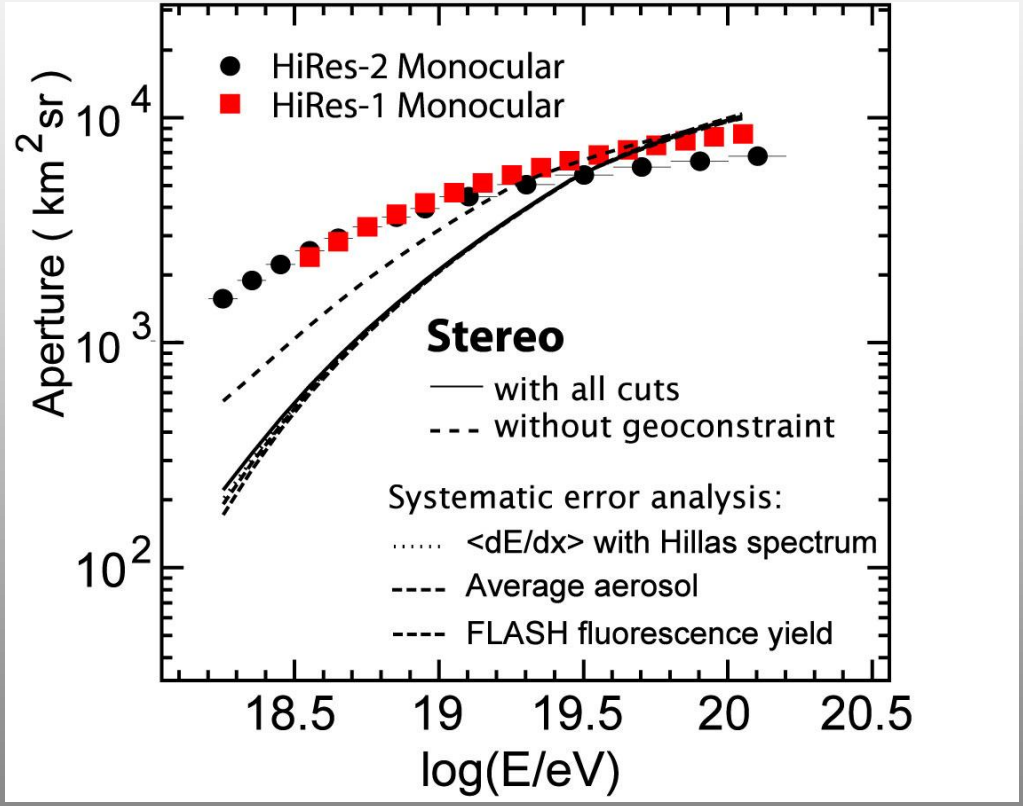

Data/MC Comparison(mono)

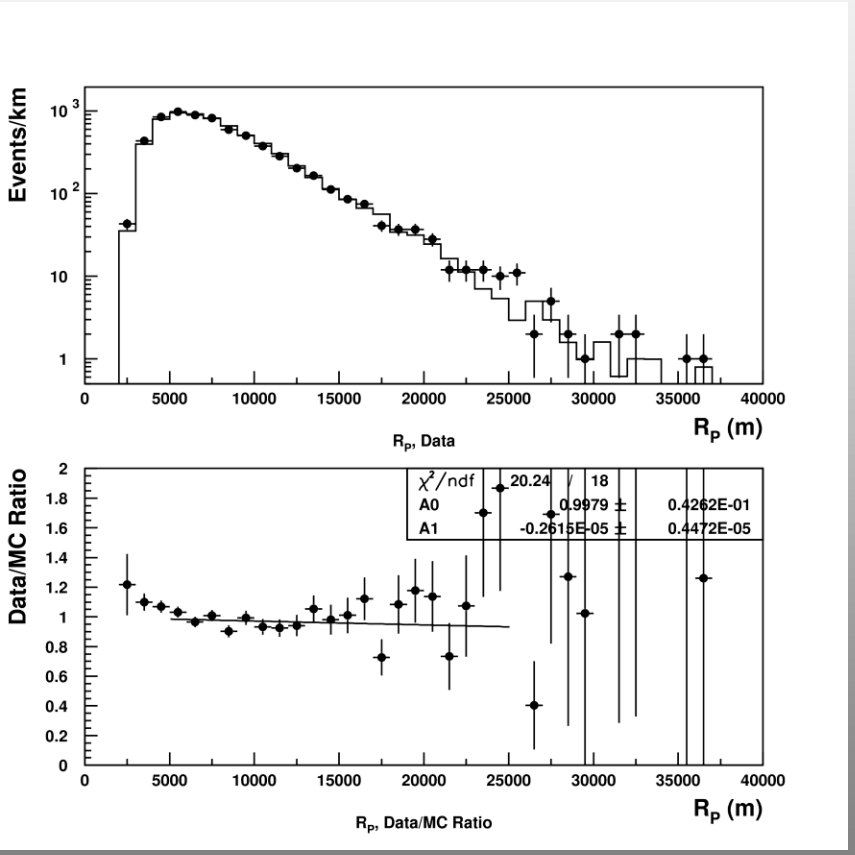

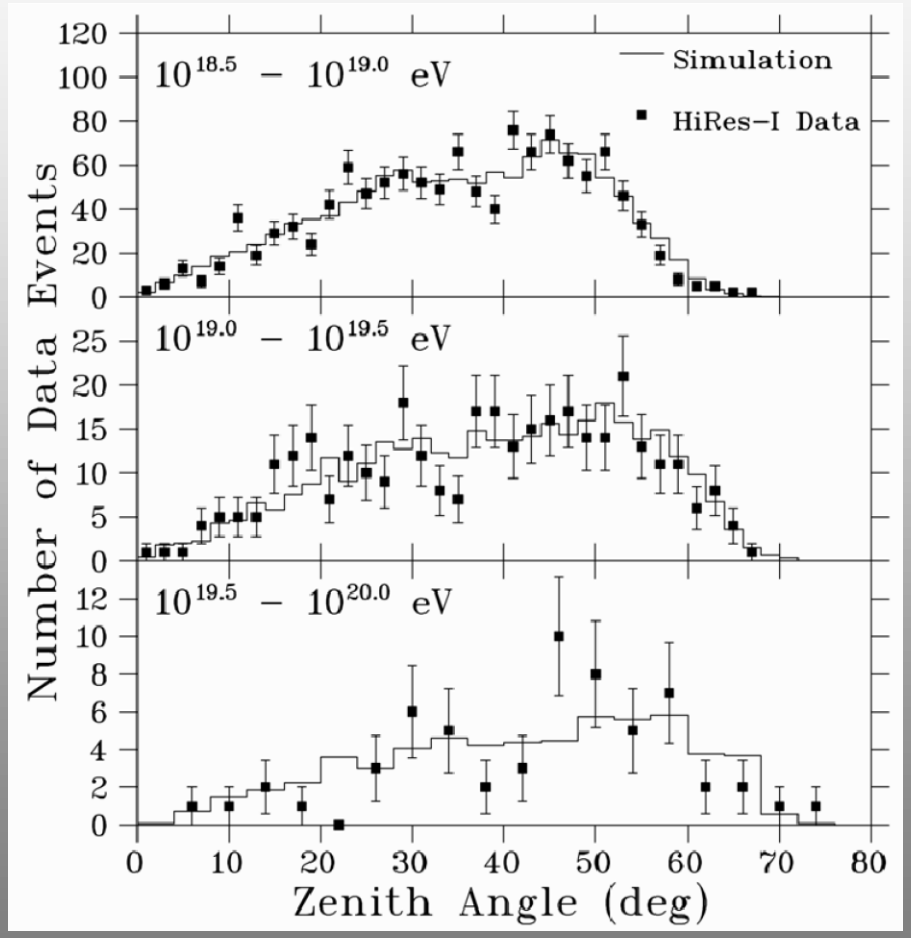

Stereo Geometrical Resolution

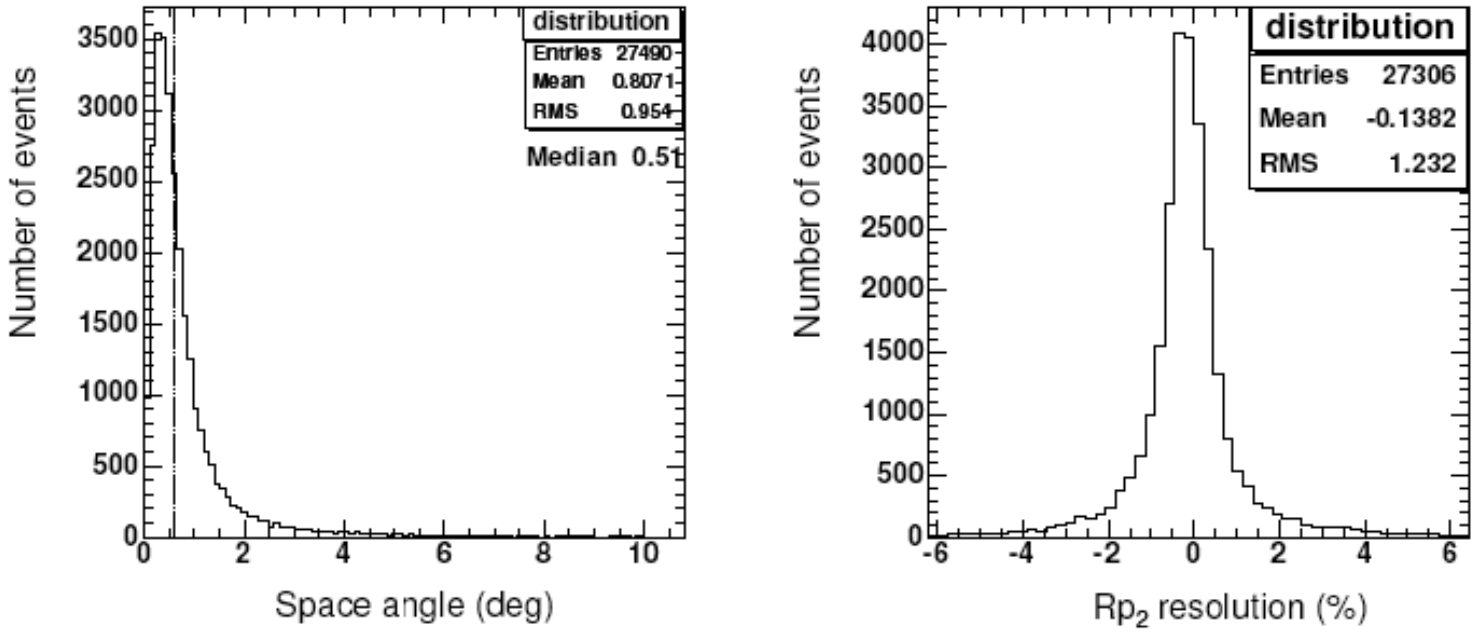

FIG. 5: Resolution functions of geometrical parameters. Left panel is the arrival direction resolution presented as the space angle between the reconstructed and known shower directions. The vertical dashed line indicates the median value of the distribution. Right panel is the R_p resolution showing a reconstruction accuracy of about 1.2%.

Stereo Energy Resolution

With Stereo Measurements, you have redundant measurements of Xmax and Energy

HR2 Energy

Resolution 15%

Systematic

17%

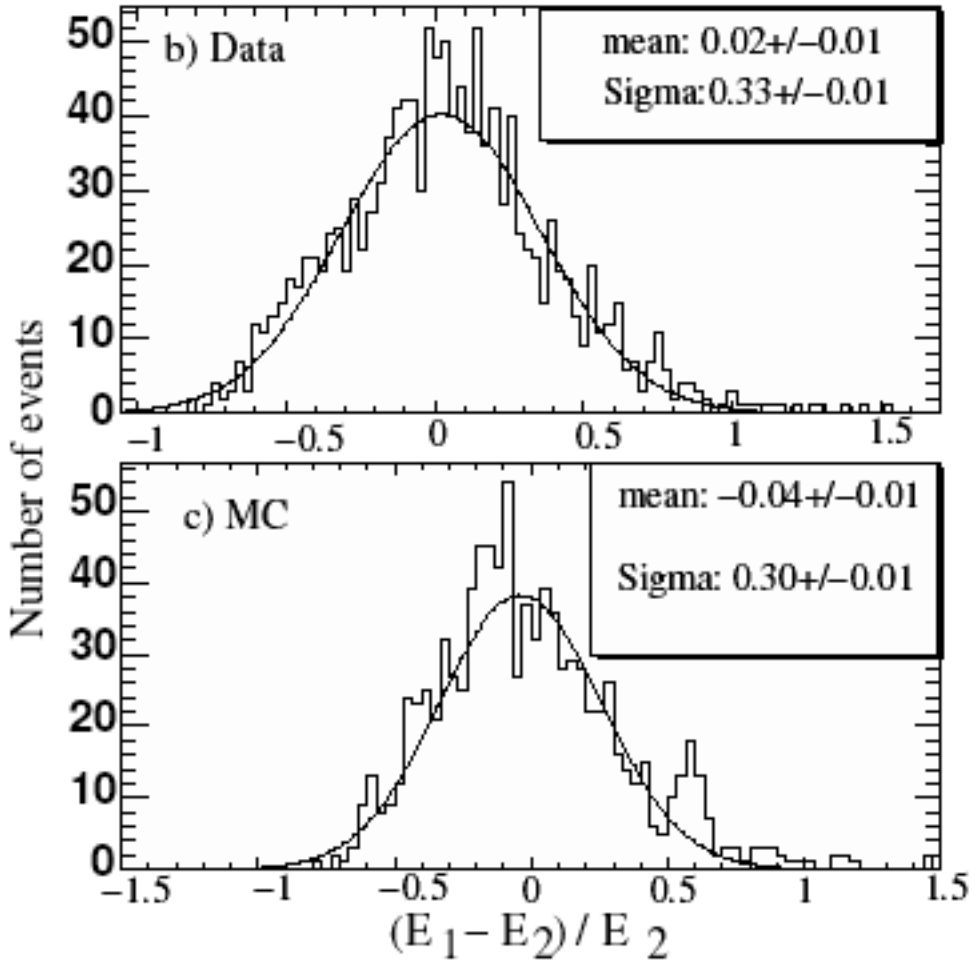

5σ Observation of the GZK Suppression (mono)

- **Broken Power Law Fits (independent data)**
  - No Break Point
    - χ^2/DOF = 162/39
  - One BP
    - χ^2/DOF = 63.0/37
    - BP = 18.63
  - Two BP's
    - χ^2/DOF = 35.1/35
    - 1st BP = 18.65 +/- .05
    - 2nd BP = 19.75 +/- .04
  - BP with Extension
    - Expect 43.2 events
    - Observe 13 events
    - Poisson probability:P(15;51.1)= 7**x10**$^{-8}$(5.3σ)

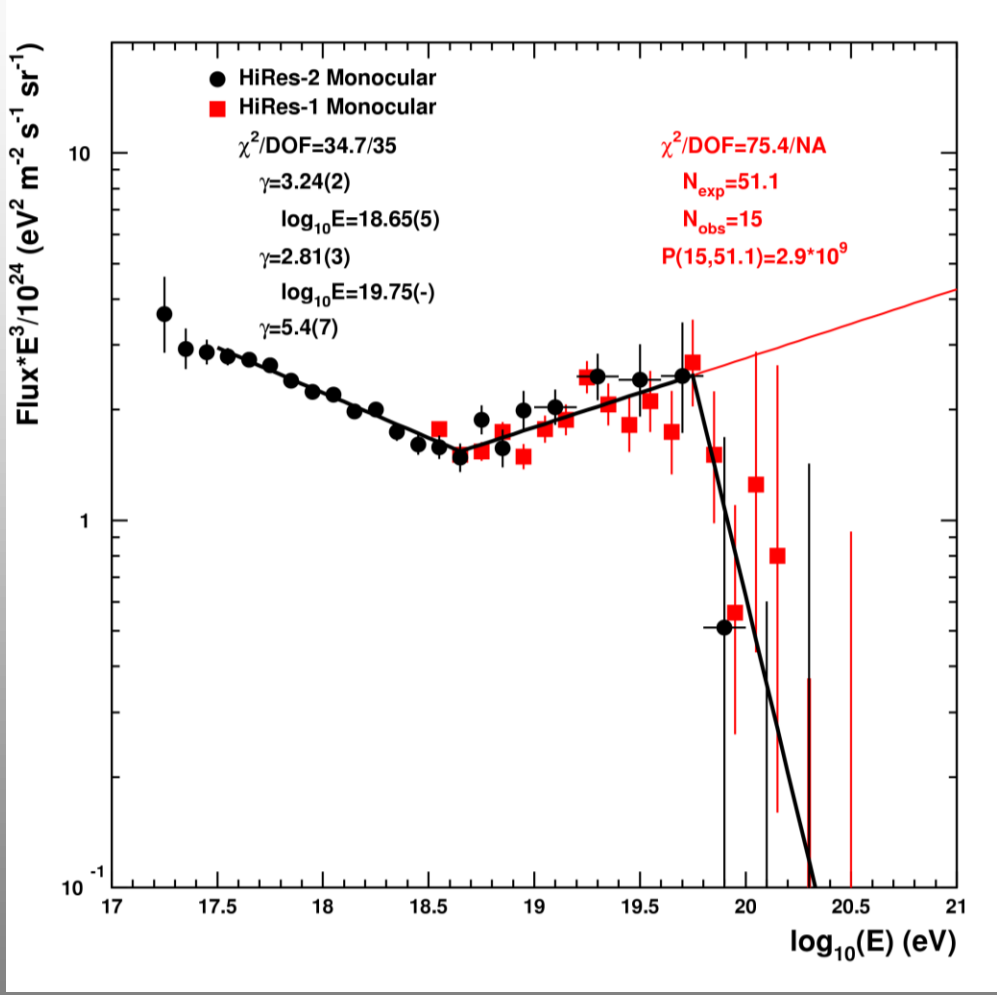

Mono and Stereo Spectra

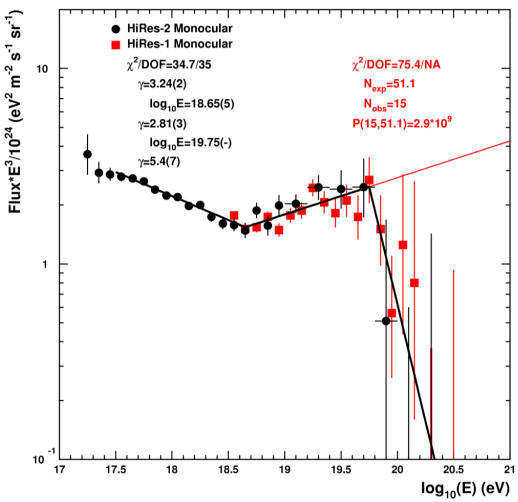

Mono – HR1 and HR2

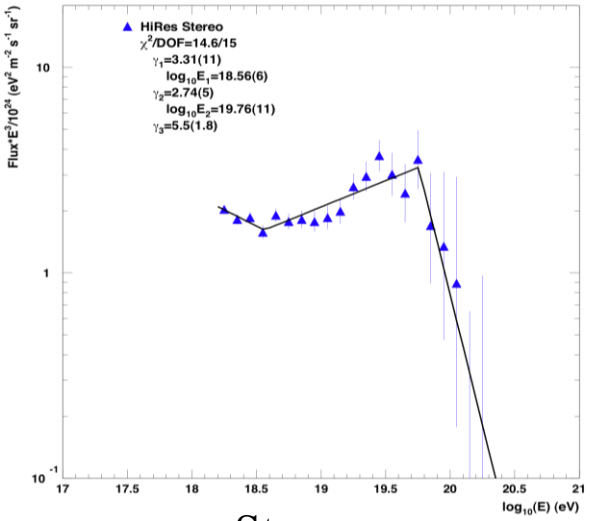

Stereo

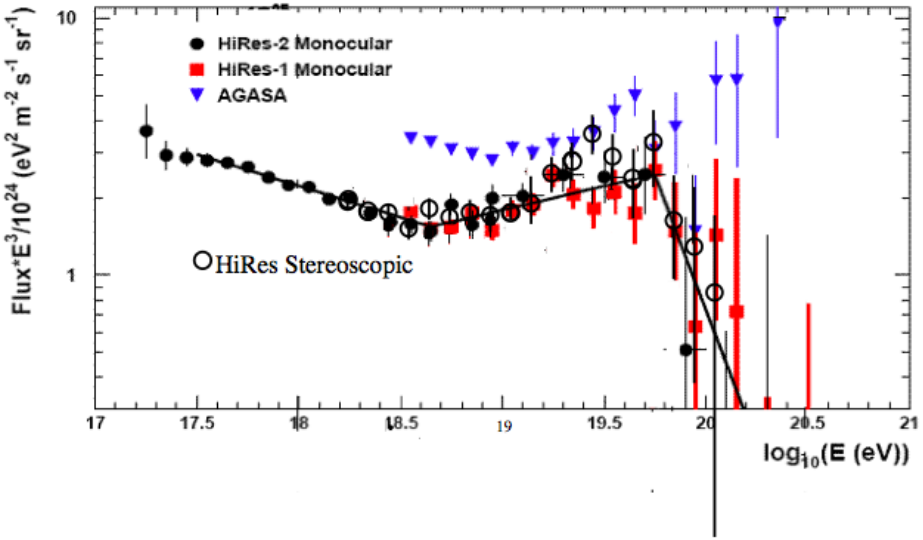

HiRes/Auger spectra comparison

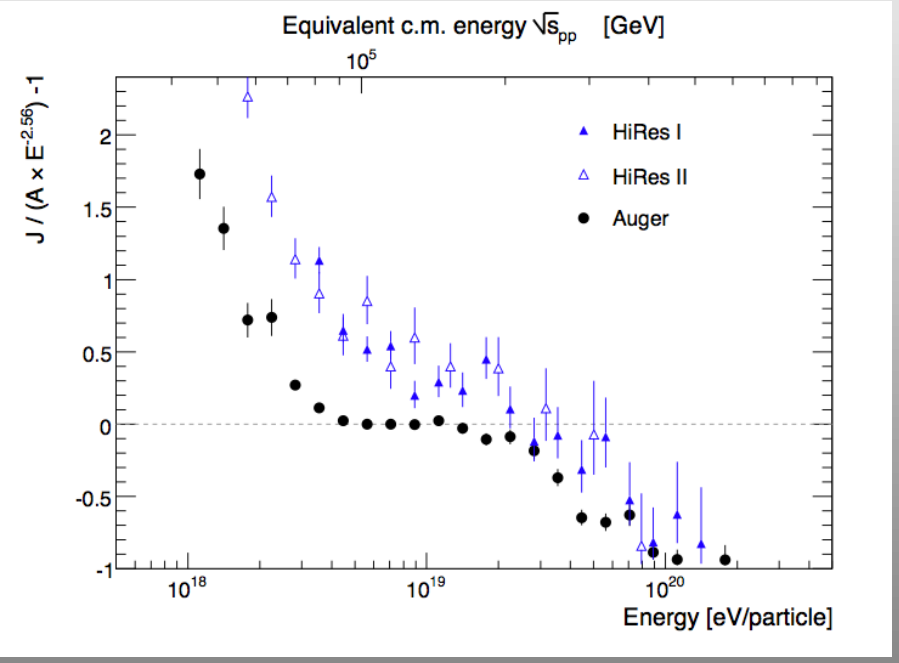

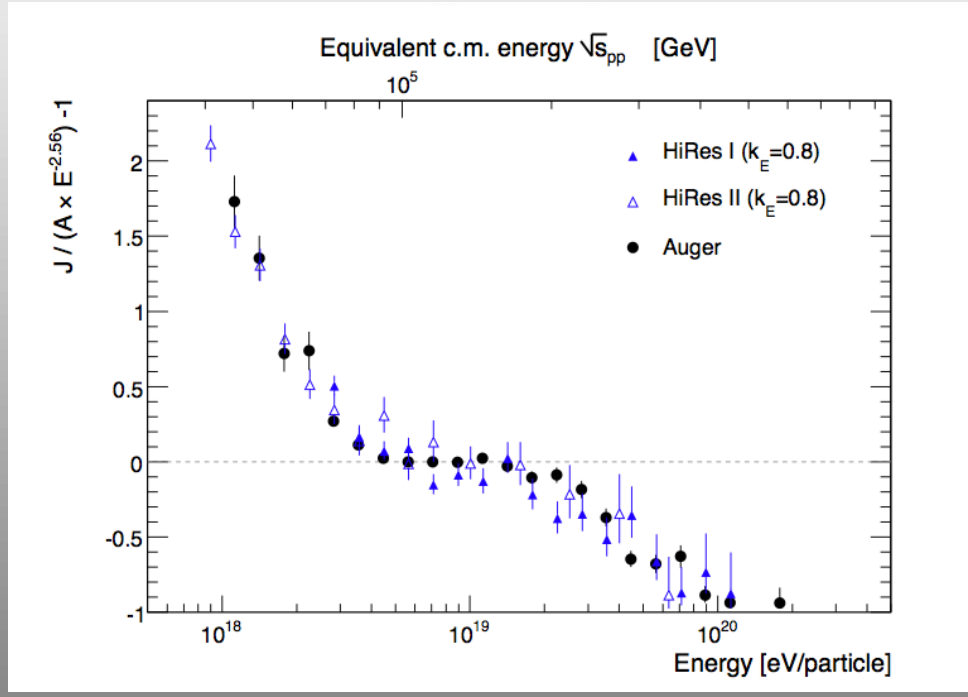

Auger confirms all spectral features of HiRes spectrum

How is Xmax defined?

- Generate CORSIKA showers in atmosphere – QGSJET01,02, Corsika etc.
- Define Xmax numerically or by fitting
- “spline” numerical fit - previously used
- Gaisser-Hillas functional form - fit to simulation and data
- Gaussian-in-age functional form
- We now use Gaussian-in-age(GIA) for both real and simulated showers

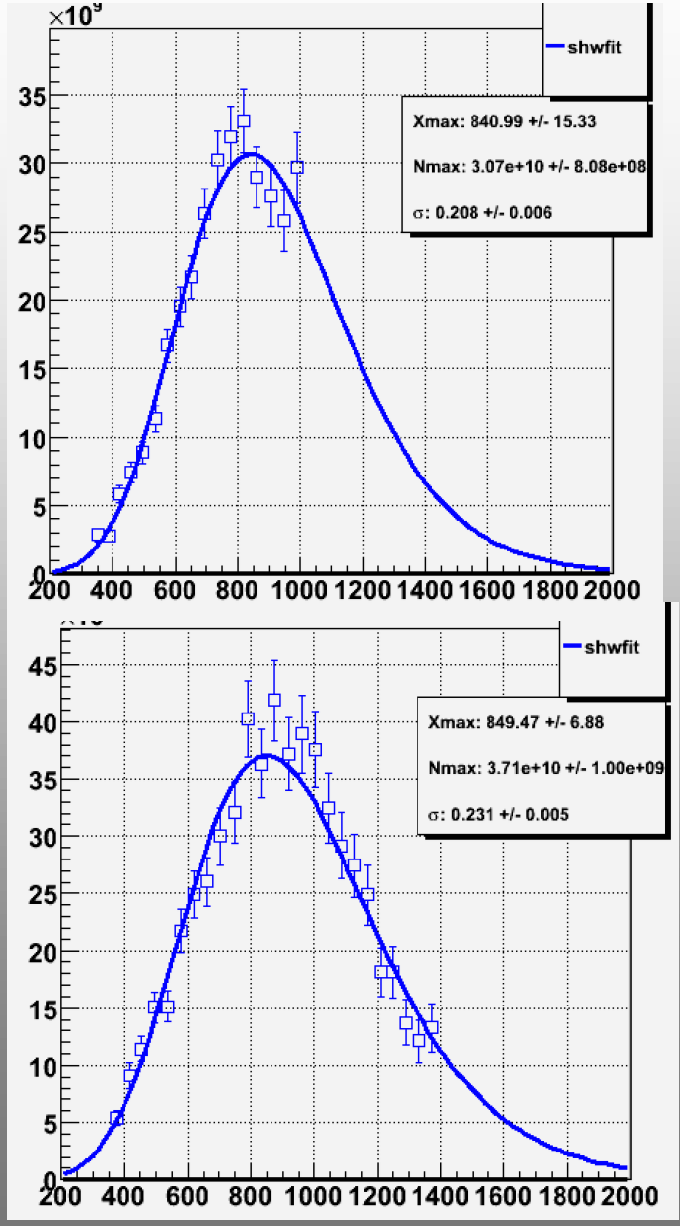

Gauss-in-age fit to two Highest energy events

Data/MC Comparisons

- Compare p and Fe simulated data with real data in all available variables
- Excellent agreement in all variables for proton composition.
- Pure Fe composition has difficulty fitting all distributions.

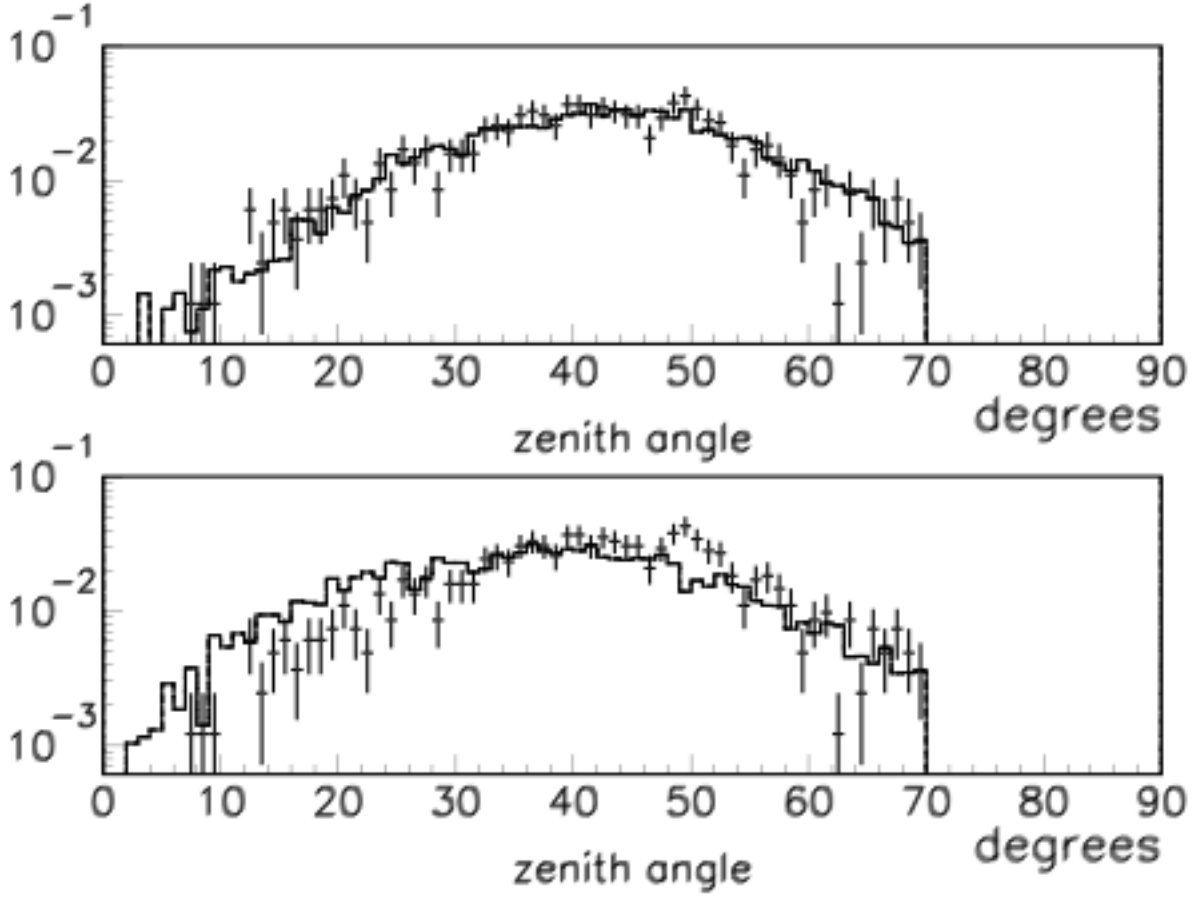

Figure 7: Data (points) Monte Carlo (histogram) comparison, distribution in zenith angle. *Top:* Comparison with QGSJET-II proton Monte Carlo. *Bottom:* Comparison with QGSJET-II iron Monte Carlo.

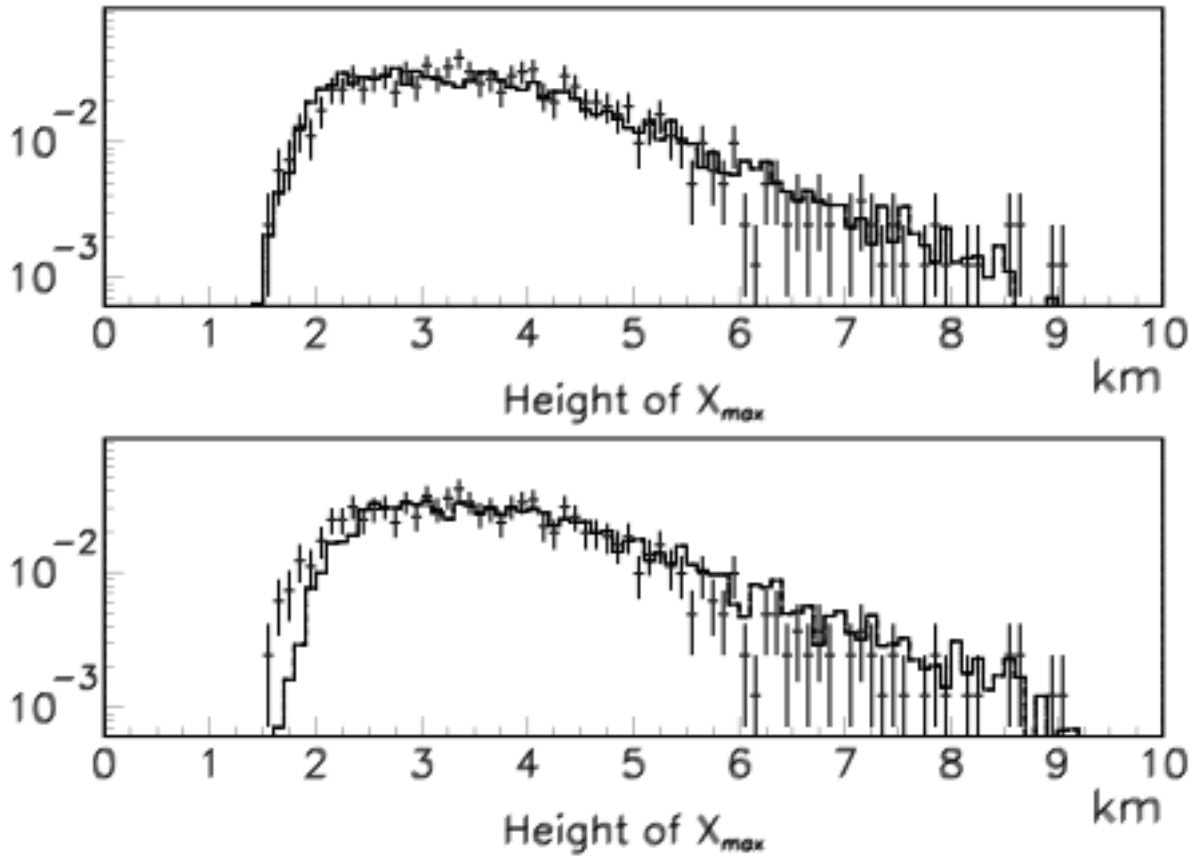

Figure 10: Data (points) Monte Carlo (histogram) comparison, distribution in height (km) of X_{max} above HiRes "ground". *Top:* Comparison with QGSJET-II proton Monte Carlo. *Bottom:* Comparison with QGSJET-II iron Monte Carlo.

Overall comparison of Xmax data with QGSJET02 p and FE

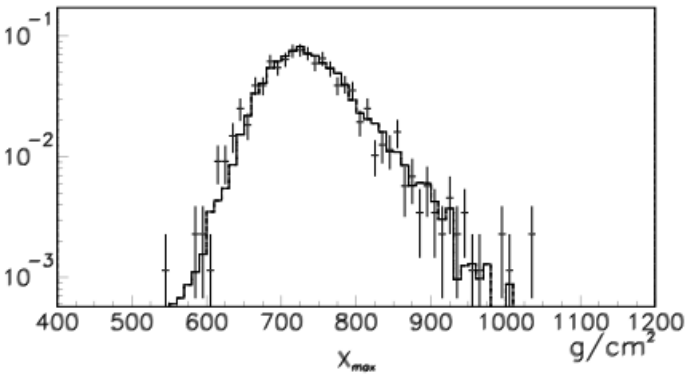

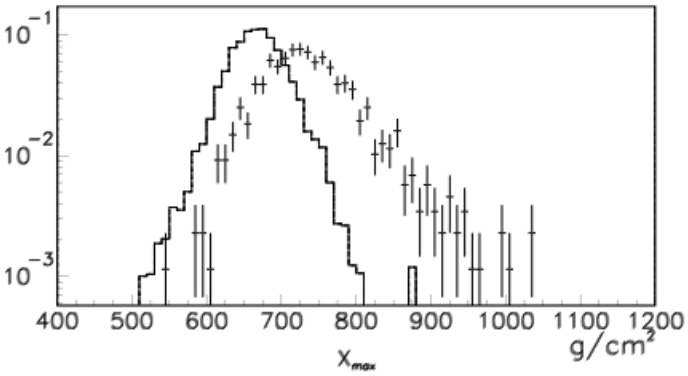

Fig. 11.— *Top:* X_{max} overlay of HiRes data (points) with QGSJET02 proton Monte Carlo airshowers after full detector simulation. *Bottom:* X_{max} overlay of HiRes data (points) with QGSJET02 iron Monte Carlo airshowers after full detector simulation.

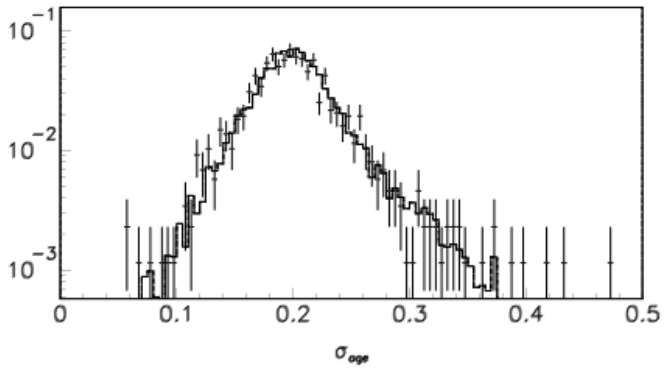

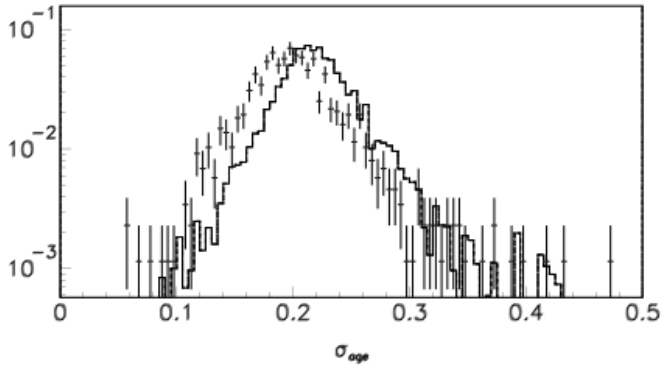

Fig. 12.— *Top:* σ_{age} overlay of HiRes data (points) with QGSJET02 proton Monte Carlo airshowers after full detector simulation. *Bottom:* σ_{age} overlay of HiRes data (points) with QGSJET02 iron Monte Carlo airshowers after full detector simulation.

Stereo Detection enables check on Xmax resolution calculation

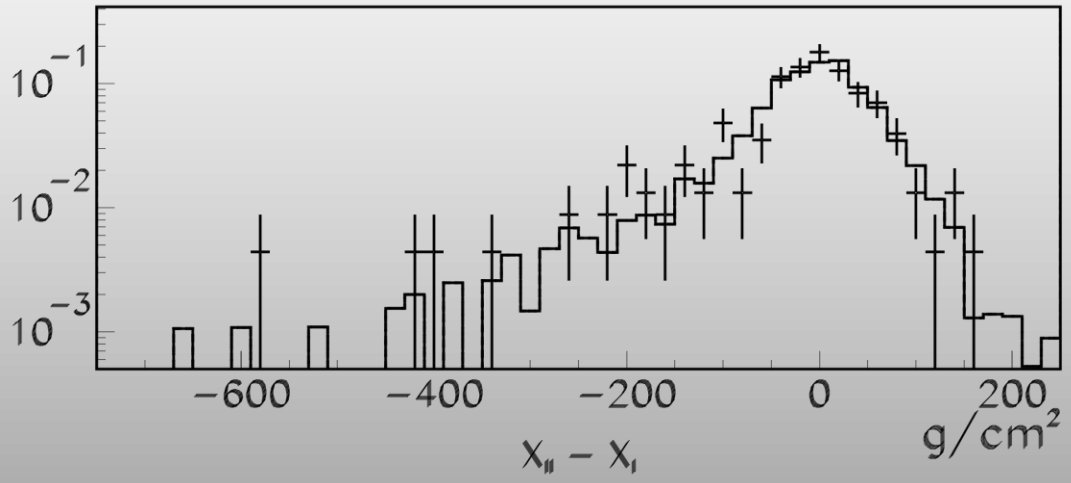

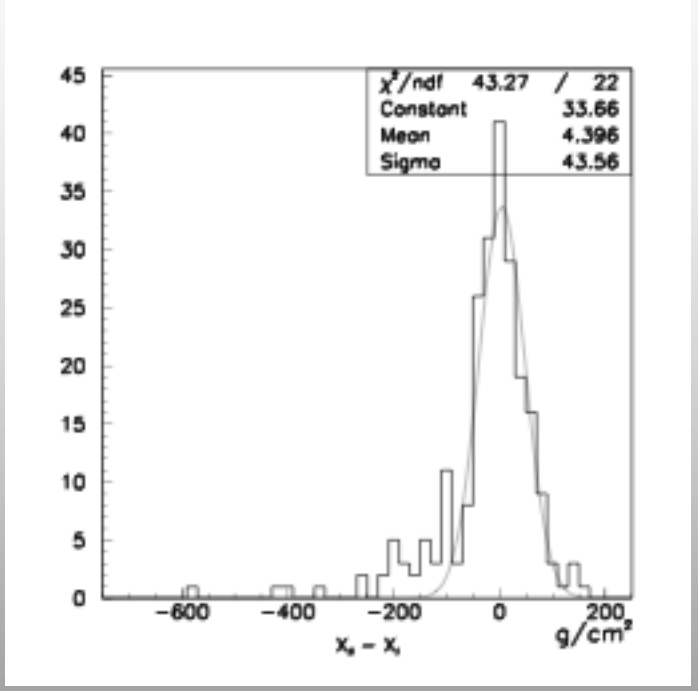

Comparison of Xmax difference with MC predictions (L)
Gaussian fit to Xmax difference (R)

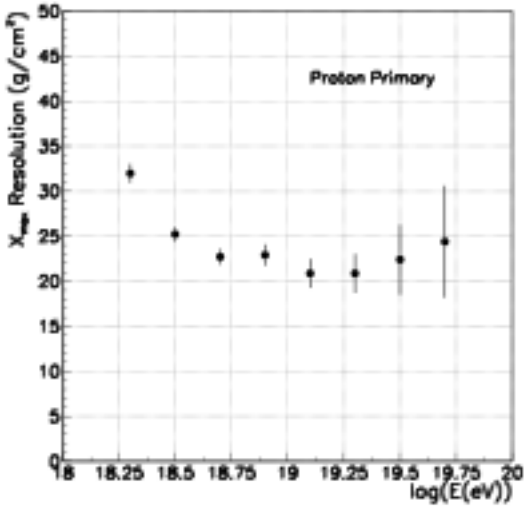

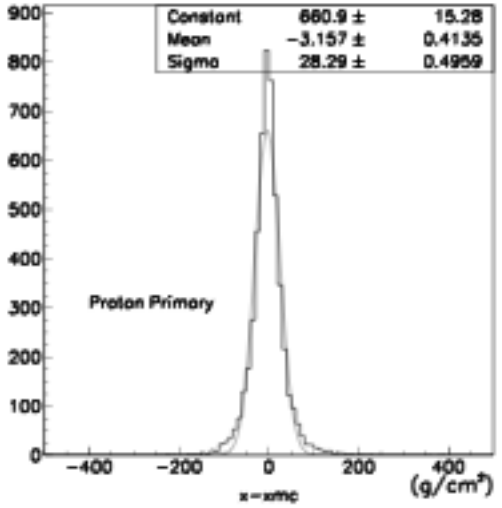

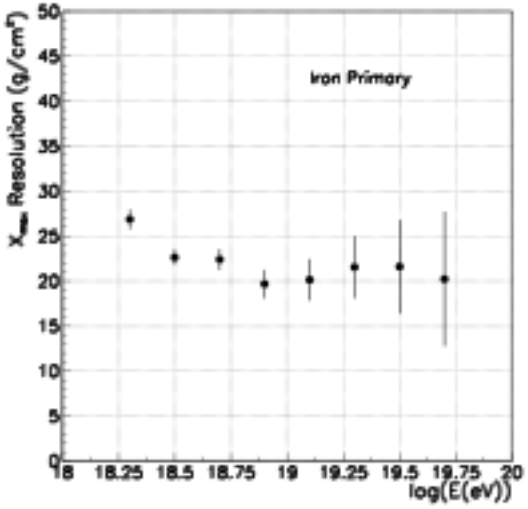

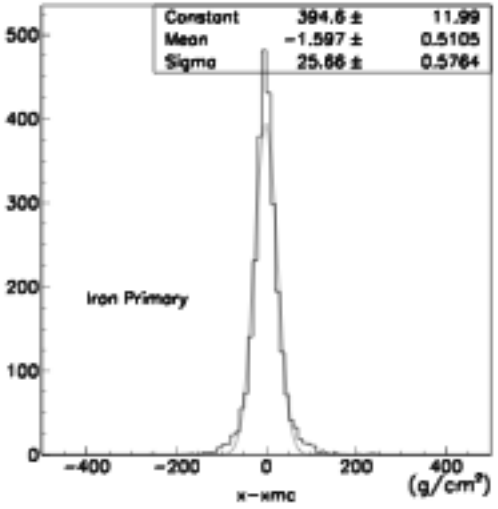

Fig. 3.— *Left:* X_{max} resolution versus $\log E$, for QGSJET2 iron showers. *Right:* Overall energy resolution, for the energies contained in this analysis, for QGSJET2 iron showers.

Reconstruction and Acceptance Bias after cuts

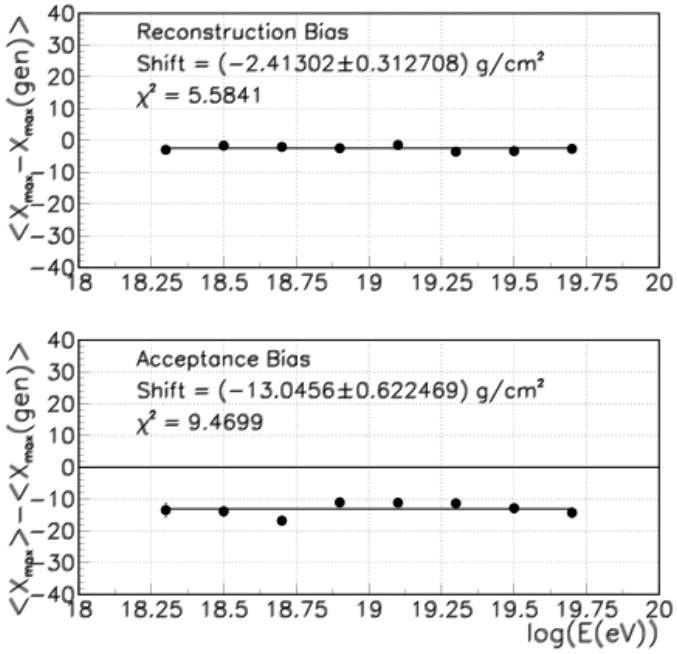

Fig. 7.— Biases to $<X_{max}>$, QGSJET02 protons, Gaussian-in-age profile fits. *Top:* Mean value of difference between reconstructed and generated X_{max}, for events which are successfully reconstructed and pass all cuts. Vertical axis is g/cm^2. Uncertainties are smaller than points shown. *Bottom:* Difference between $<X_{max}>$ for reconstructed events and $<X_{max}>$ for *all* showers in the thrown shower library.

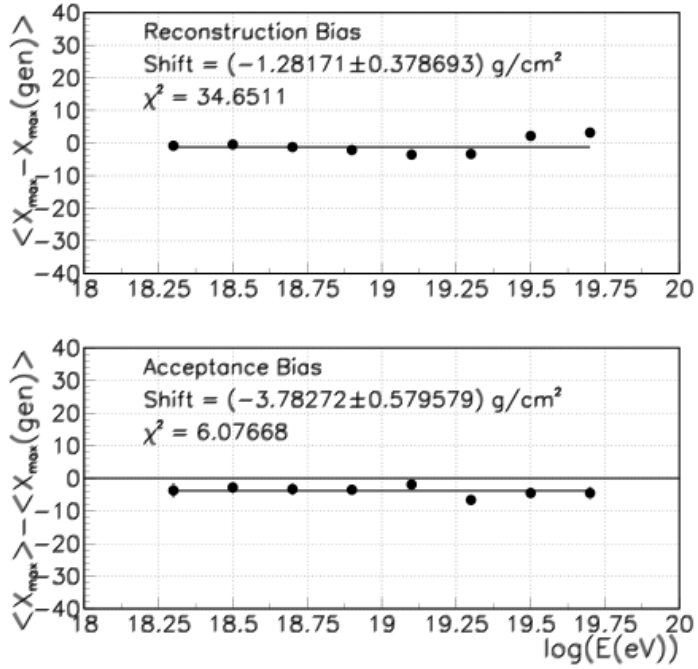

Fig. 10.— Biases to $<X_{max}>$, QGSJET02 iron, Gaussian-in-age profile fits. *Top:* Mean value of difference between reconstructed and generated X_{max}, for events which are successfully reconstructed and pass all cuts. Vertical axis is g/cm^2. Uncertainties are smaller than points shown. *Bottom:* Difference between $<X_{max}>$ for reconstructed events and $<X_{max}>$ for *all* showers in the thrown shower library.

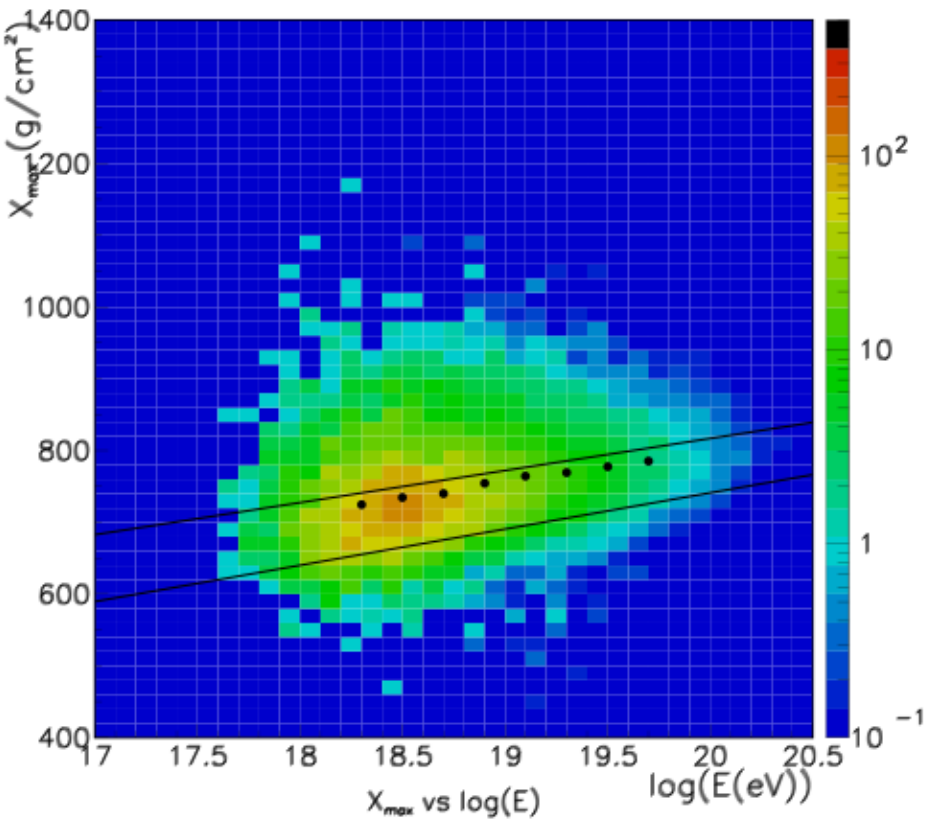

Fig. 15.— Scatter plot of X_{max} versus log E for QGSET02 proton Monte Carlo, after full detector simulation. Points represent the average X_{max} in each energy bin. Also superimposed are QGSJET02 proton (top) and iron (bottom) "rails" taken from simulated airshower events prior to detector effects. See also Figure 1. Final energy cuts have not yet been applied.

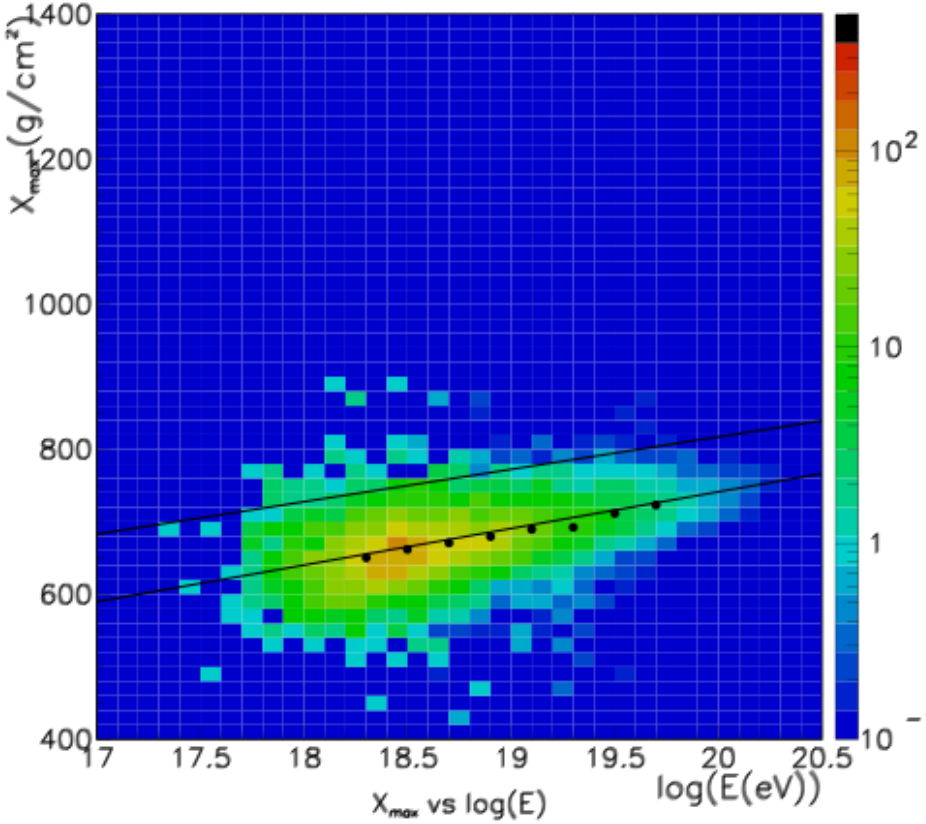

Fig. 16.— Scatter plot of X_{max} versus log E for QGSET02 iron Monte Carlo, after full detector simulation. Points represent the average X_{max} in each energy bin. Also superimposed are QGSJET02 proton (top) and iron (bottom) "rails" taken from simulated airshower events prior to detector effects. See also Figure 1. Final energy cuts have not yet been applied.

QGSJET02 p and Fe Xmax plots, full detector simulation

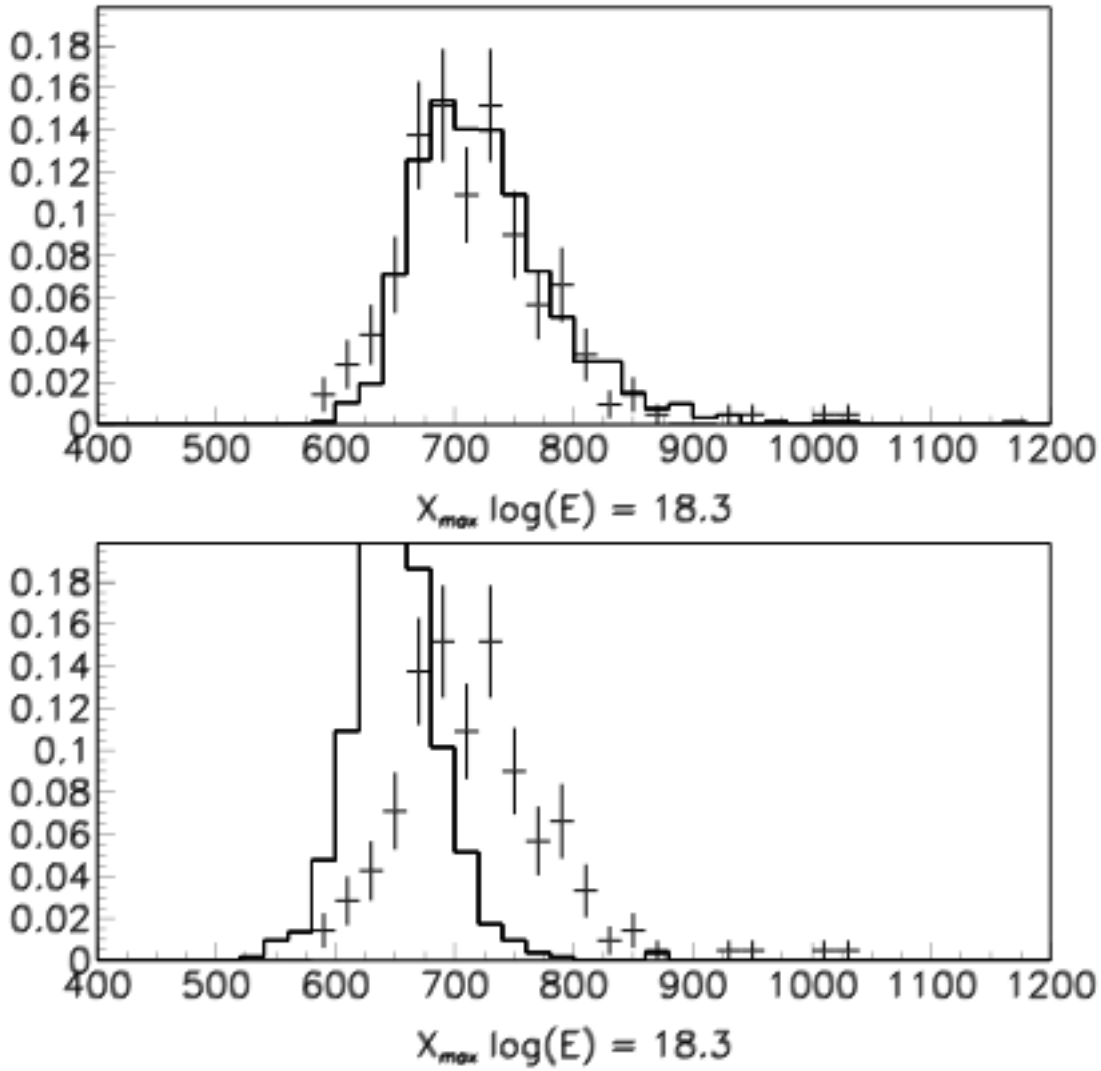

Figure 12: Data (points) compared to QGSJET-II Monte Carlo (histograms) X_{max} distributions, in bin centered at $\log E = 18.3$. Top plot is comparison with pure proton MC, bottom with pure iron MC.

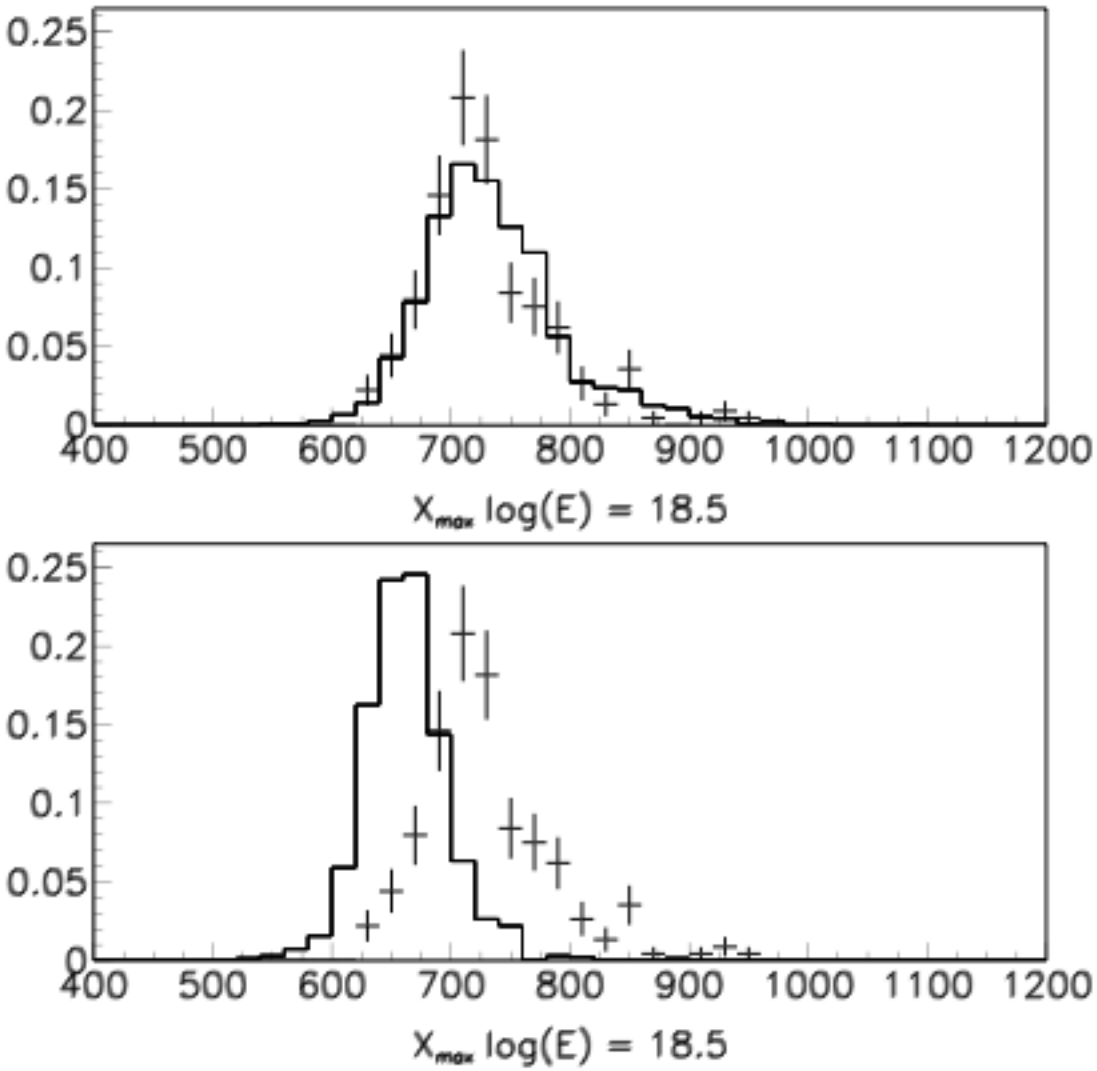

Figure 13: Data (points) compared to QGSJET-II Monte Carlo (histograms) X_{max} distributions, in bin centered at $\log E = 18.5$. Top plot is comparison with pure proton MC, bottom with pure iron MC.

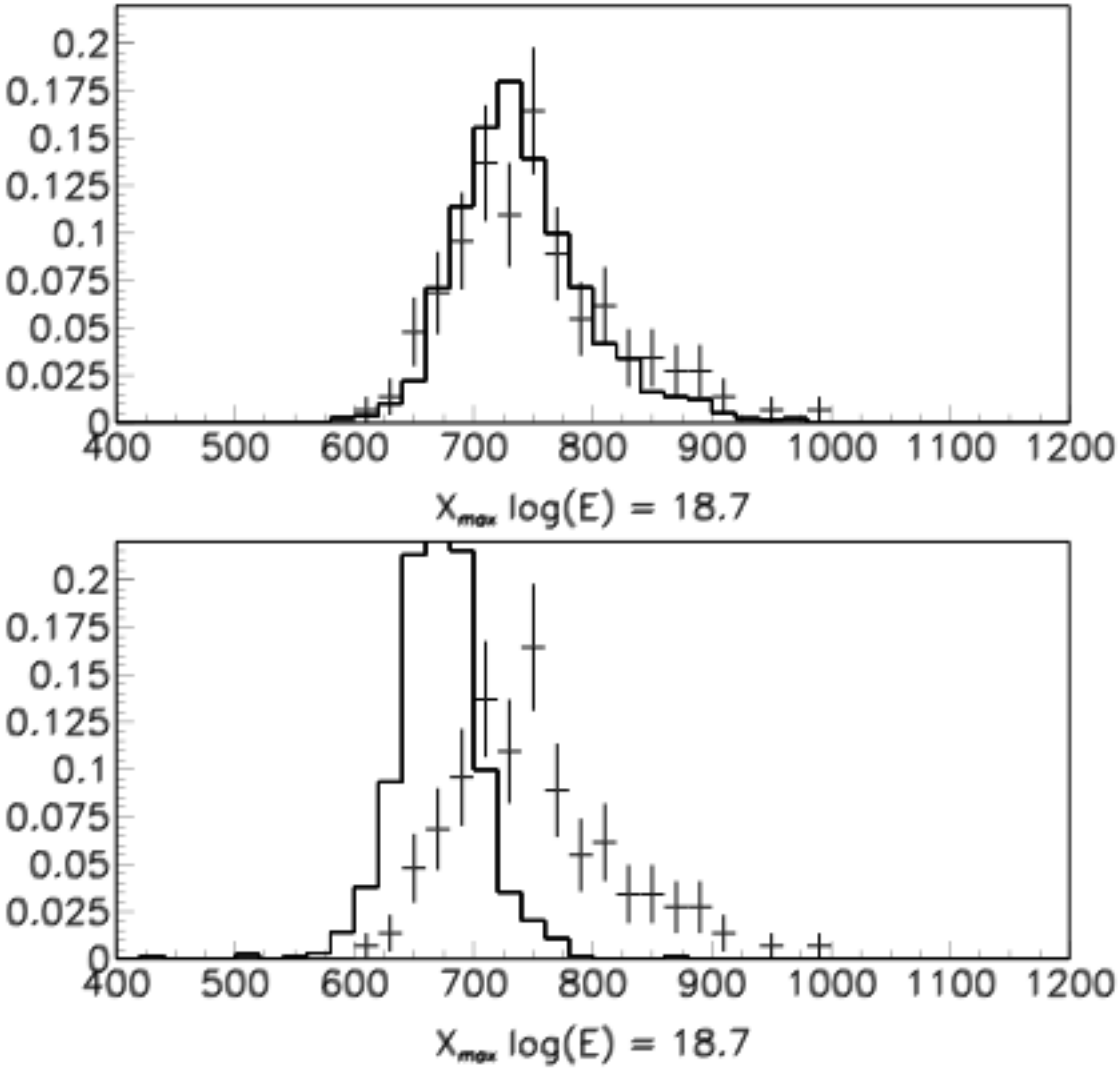

Figure 14: Data (points) compared to QGSJET-II Monte Carlo (histograms) X_{max} distributions, in bin centered at $\log E = 18.7$. Top plot is comparison with pure proton MC, bottom with pure iron MC.

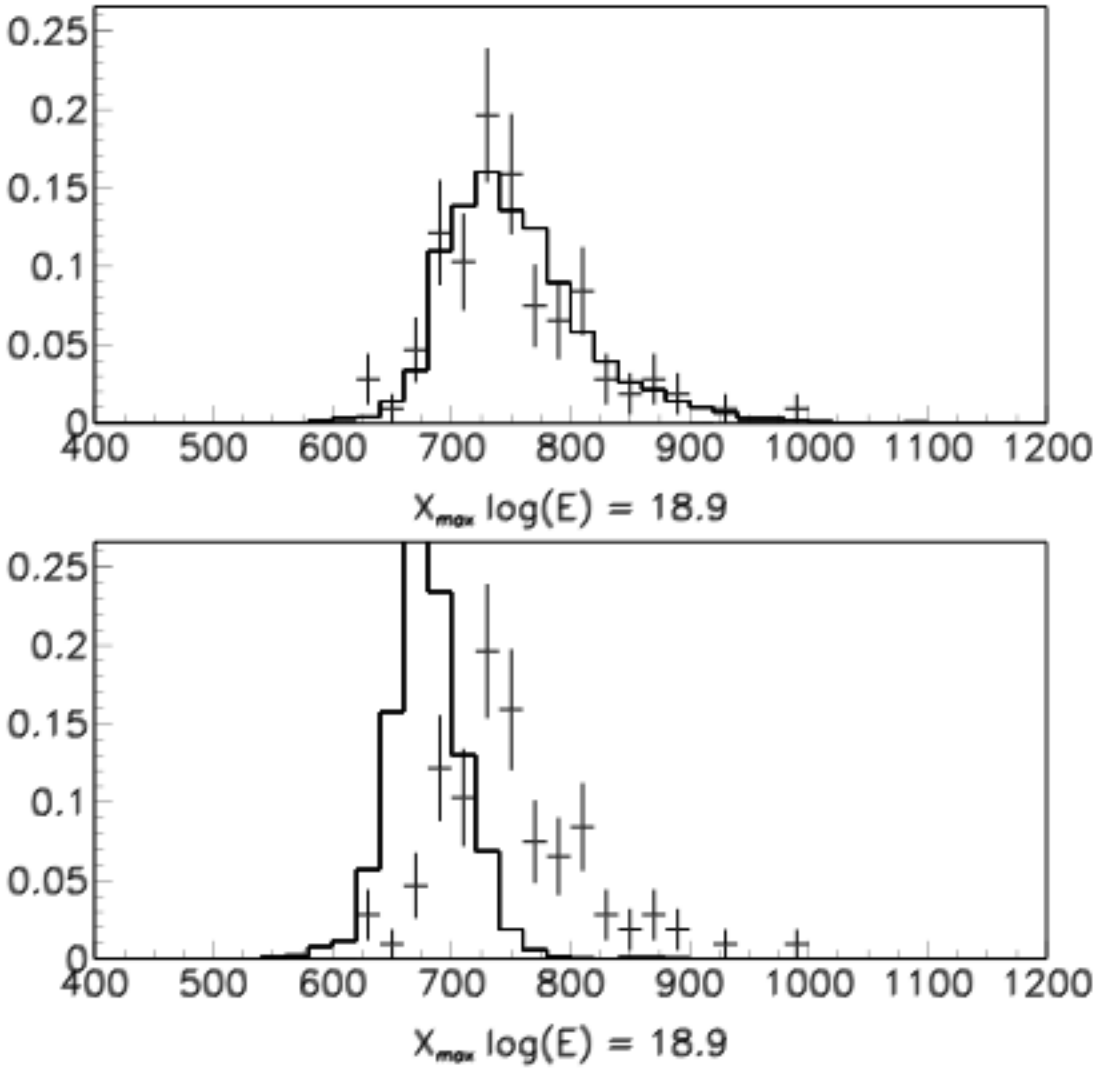

Figure 15: Data (points) compared to QGSJET-II Monte Carlo (histograms) X_{max} distributions, in bin centered at $\log E = 18.9$. Top plot is comparison with pure proton MC, bottom with pure iron MC.

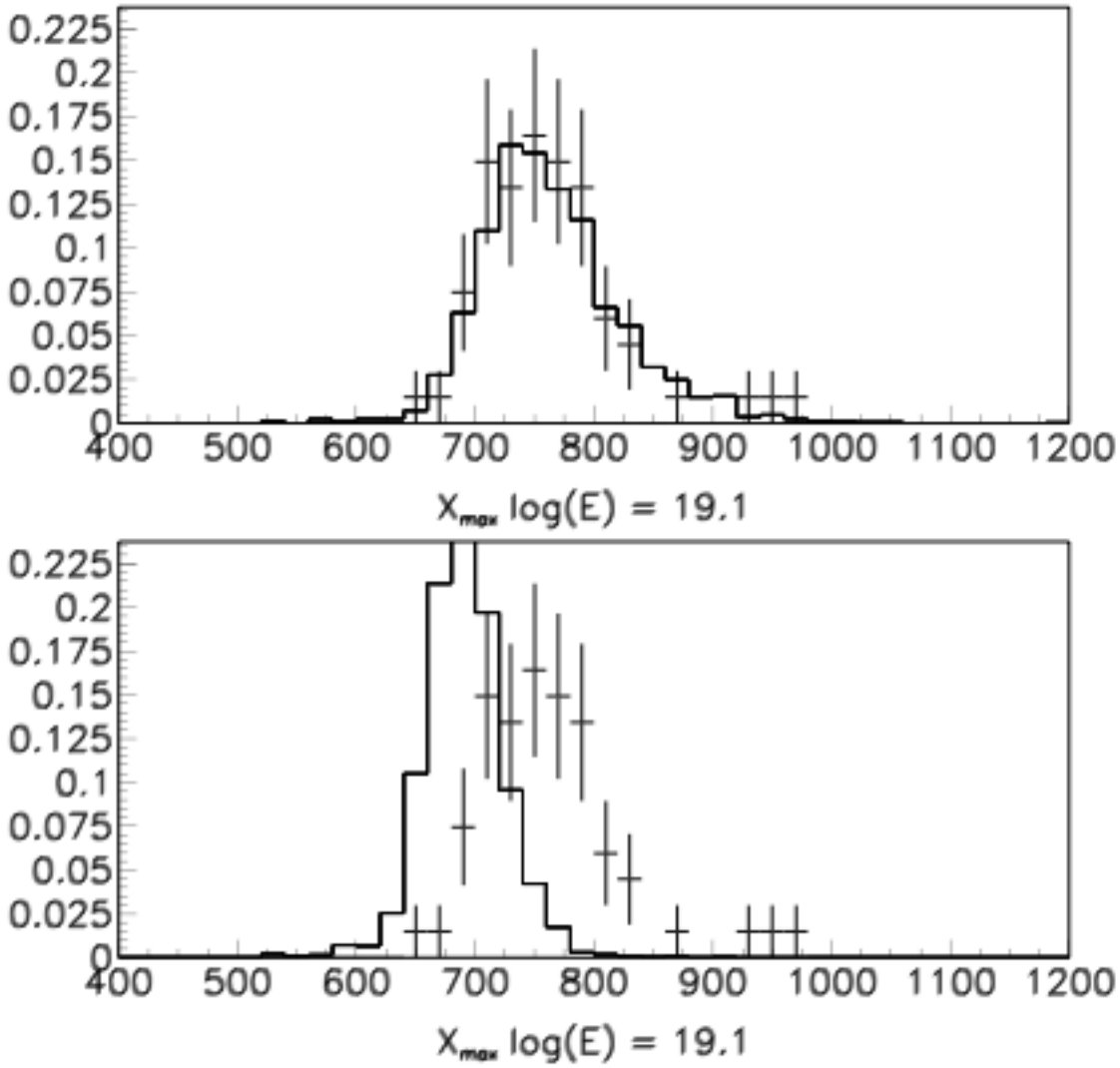

Figure 16: Data (points) compared to QGSJET-II Monte Carlo (histograms) X_{max} distributions, in bin centered at $\log E = 19.1$. Top plot is comparison with pure proton MC, bottom with pure iron MC.

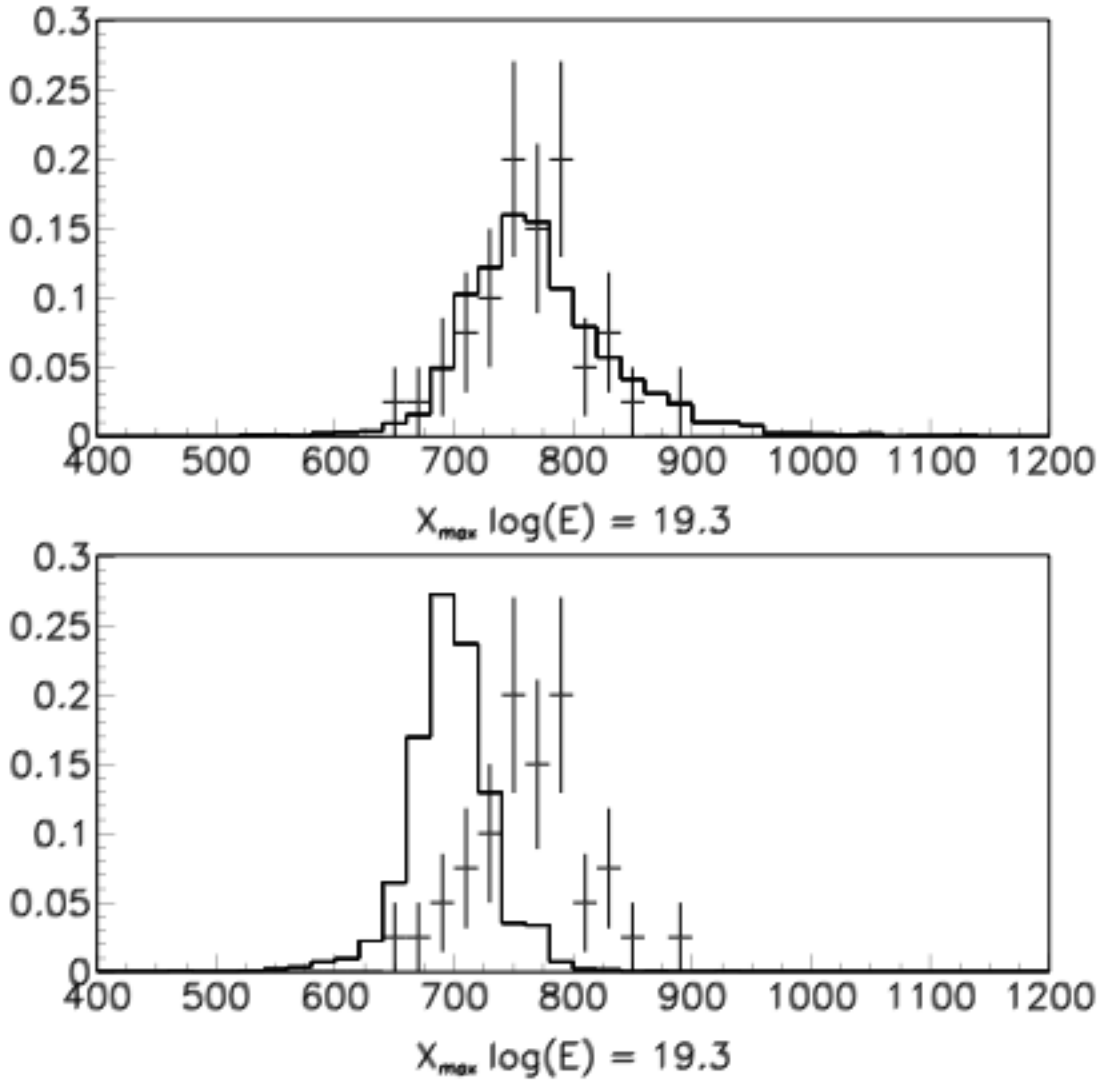

Figure 17: Data (points) compared to QGSJET-II Monte Carlo (histograms) X_{max} distributions, in bin centered at $\log E = 19.3$. Top plot is comparison with pure proton MC, bottom with pure iron MC.

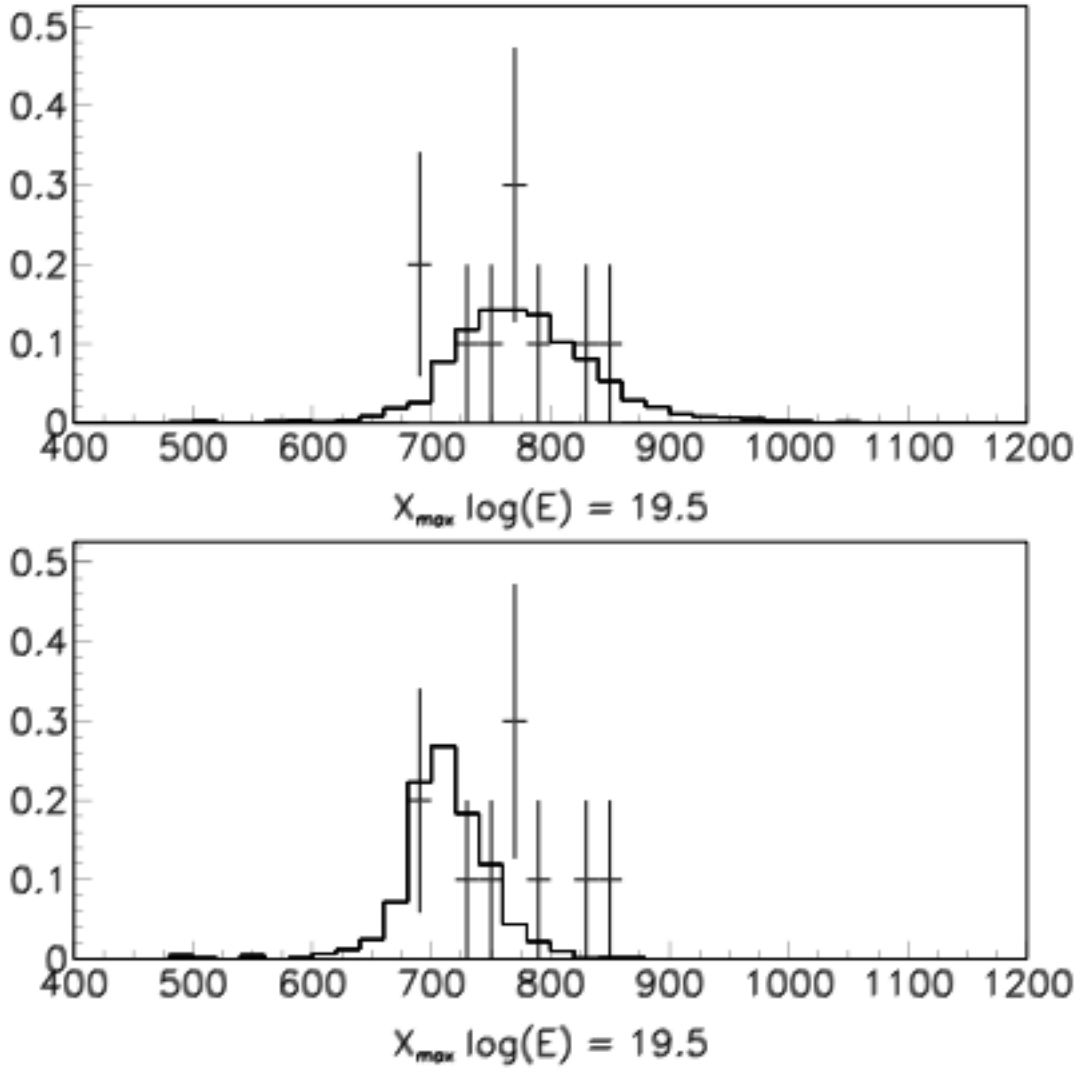

Figure 18: Data (points) compared to QGSJET-II Monte Carlo (histograms) X_{max} distributions, in bin centered at $\log E = 19.5$. Top plot is comparison with pure proton MC, bottom with pure iron MC.

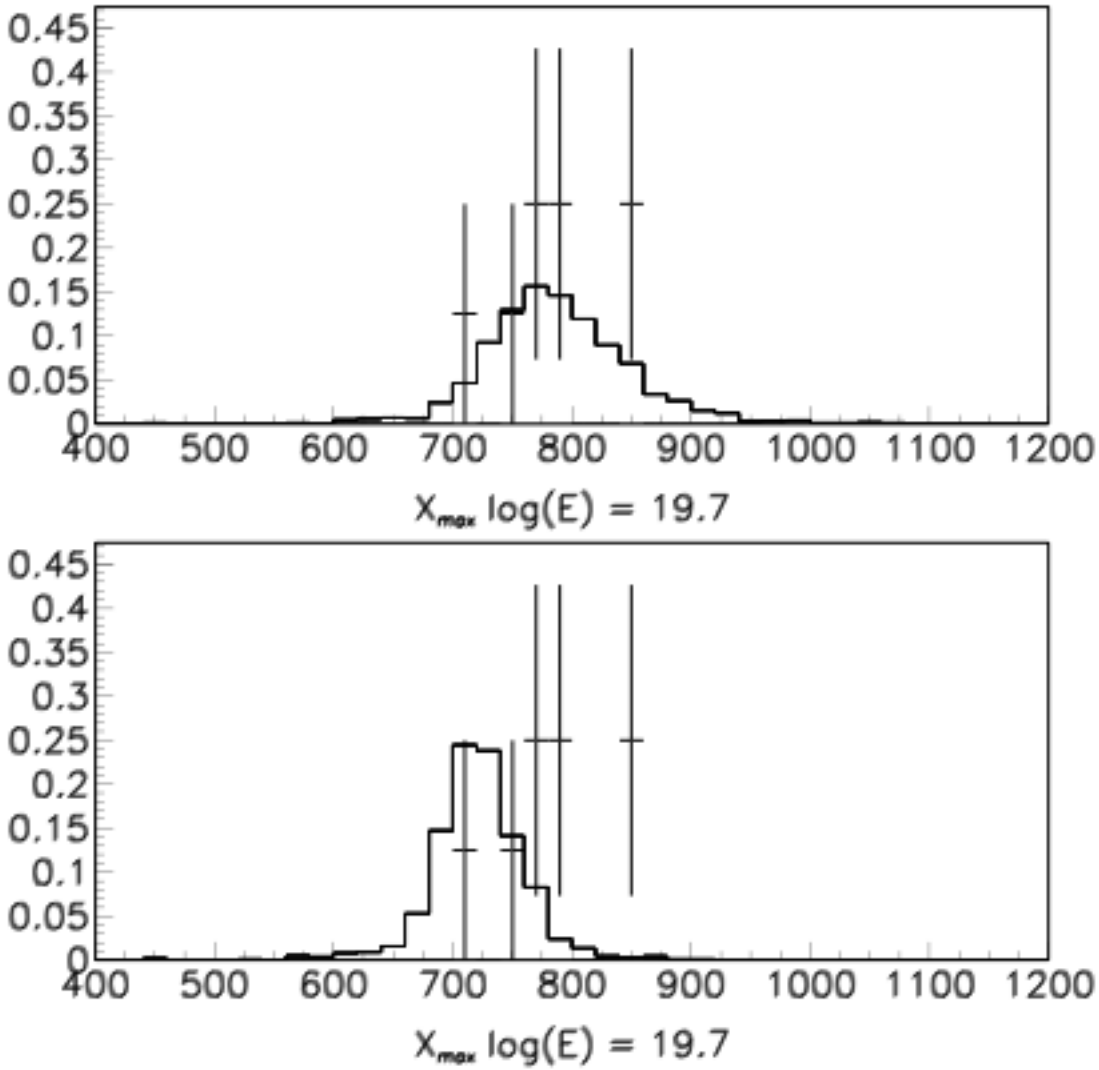

Figure 19: Data (points) compared to QGSJET-II Monte Carlo (histograms) X_{max} distributions, in bin centered at $\log E = 19.7$. Top plot is comparison with pure proton MC, bottom with pure iron MC.

HiRes Elongation Rate – Simulated data includes all Detector resolution and bias effects.

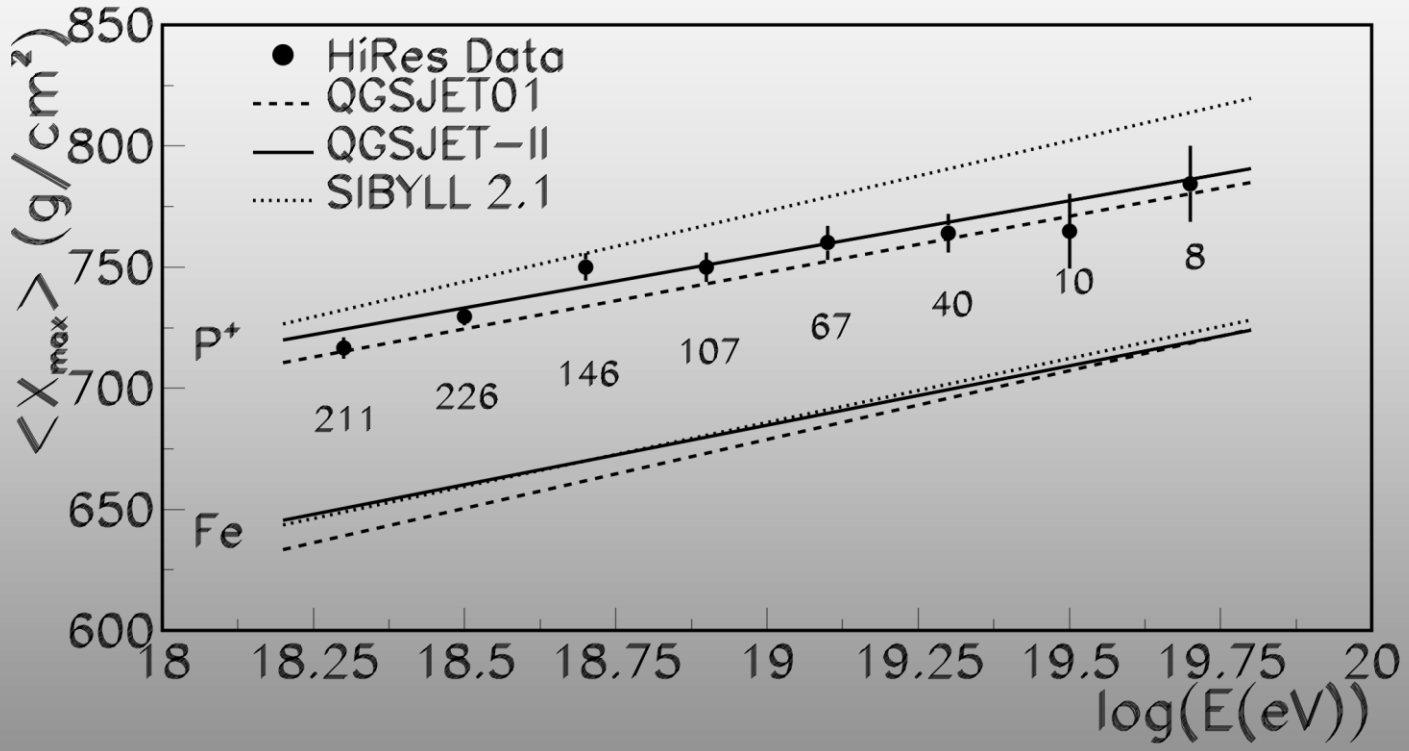

Chisq = 6.9/8 degrees of freedom for QGSJET-II
Elongation rate = 47.9 +/- 6 (stat) +/- 2.7 (sys) gm/cm2/dec

X_{max} distribution.

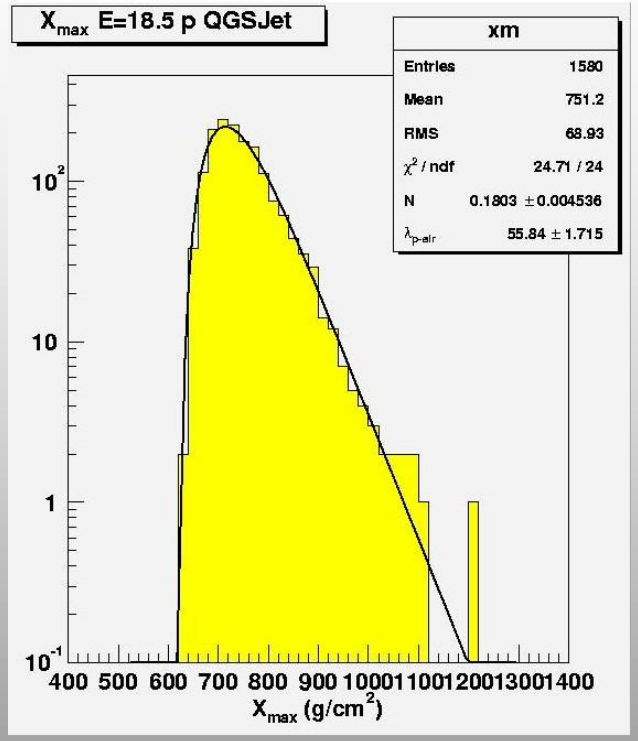

- Xmax distribution is considered as a convolution of X1 and X' distributions.

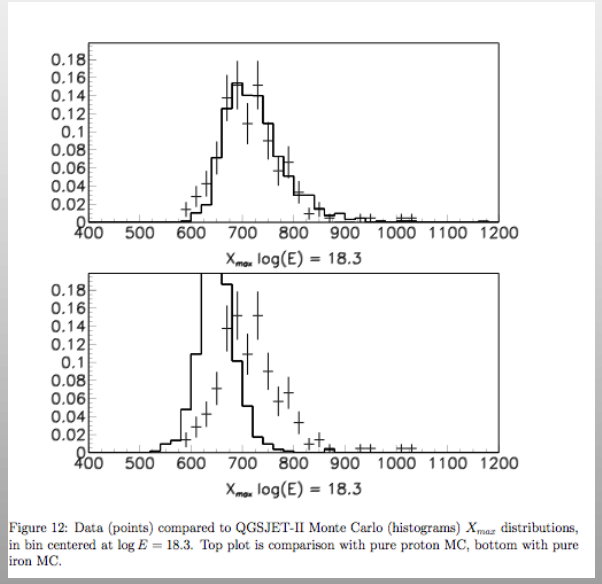

Figure 12: Data (points) compared to QGSJET-II Monte Carlo (histograms) X_{max} distributions, in bin centered at $\log E = 18.3$. Top plot is comparison with pure proton MC, bottom with pure iron MC.

$$P_m(x_m) = \left(e^{\frac{x_1}{\lambda_{p-air}}} \right) \otimes \left(\left[\frac{x_{max} - x_{peak} - x_1 + \Lambda'\alpha}{e} \right]^{\alpha} e^{\frac{x_{max} - x_1 - x_{peak}}{\Lambda'}} \right) = N \int_0^{x_m - x_{peak} + \Lambda'\alpha} e^{\frac{-x_1}{\lambda_{p-Air}}} \left[\frac{x_{max} - x_{peak} - x_1 + \Lambda'\alpha}{e} \right]^{\alpha} e^{-\frac{x_{max} - x_1 - x_{peak}}{\Lambda'}} dx_1;$$

HiRes 2007 Measurement.

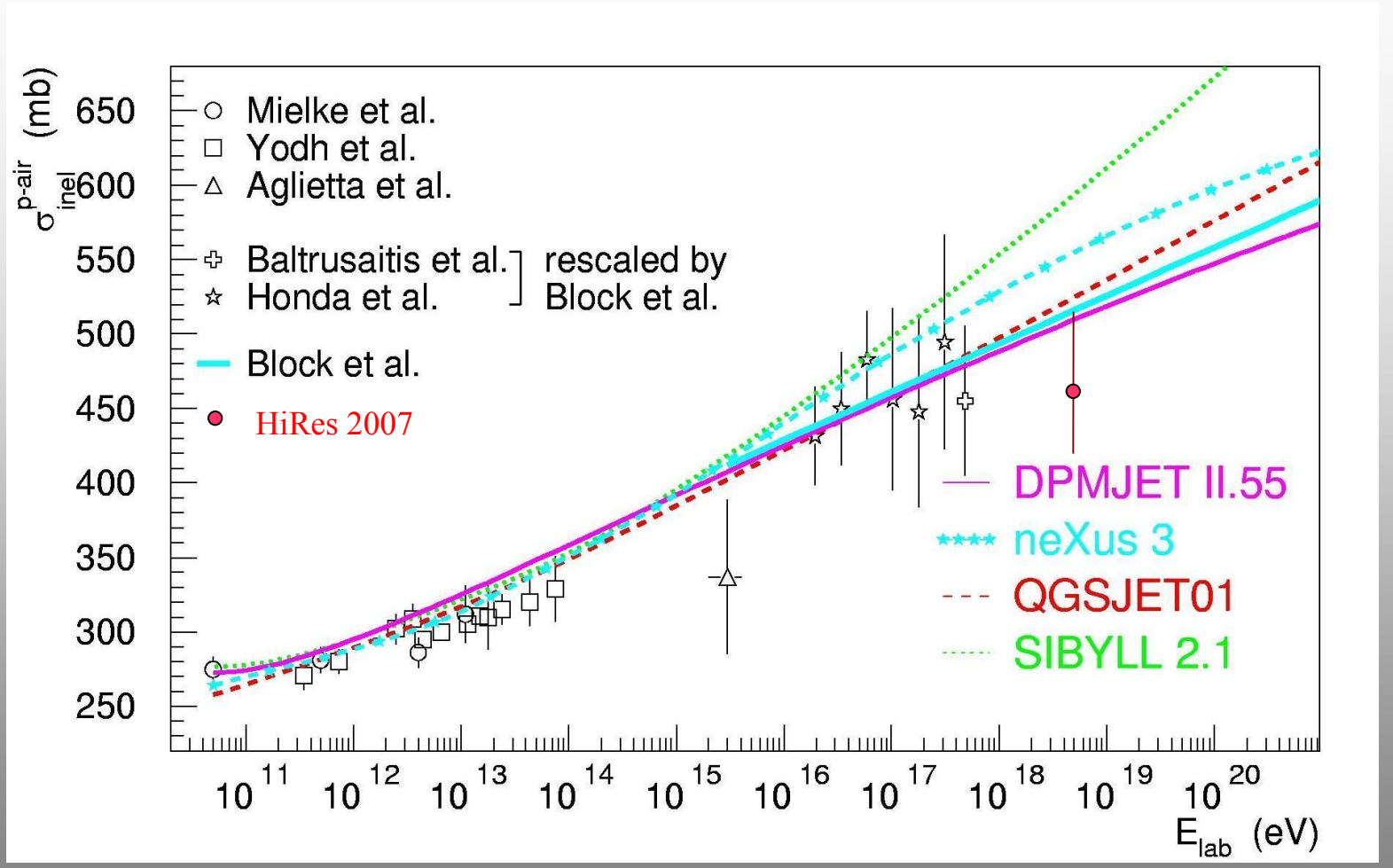

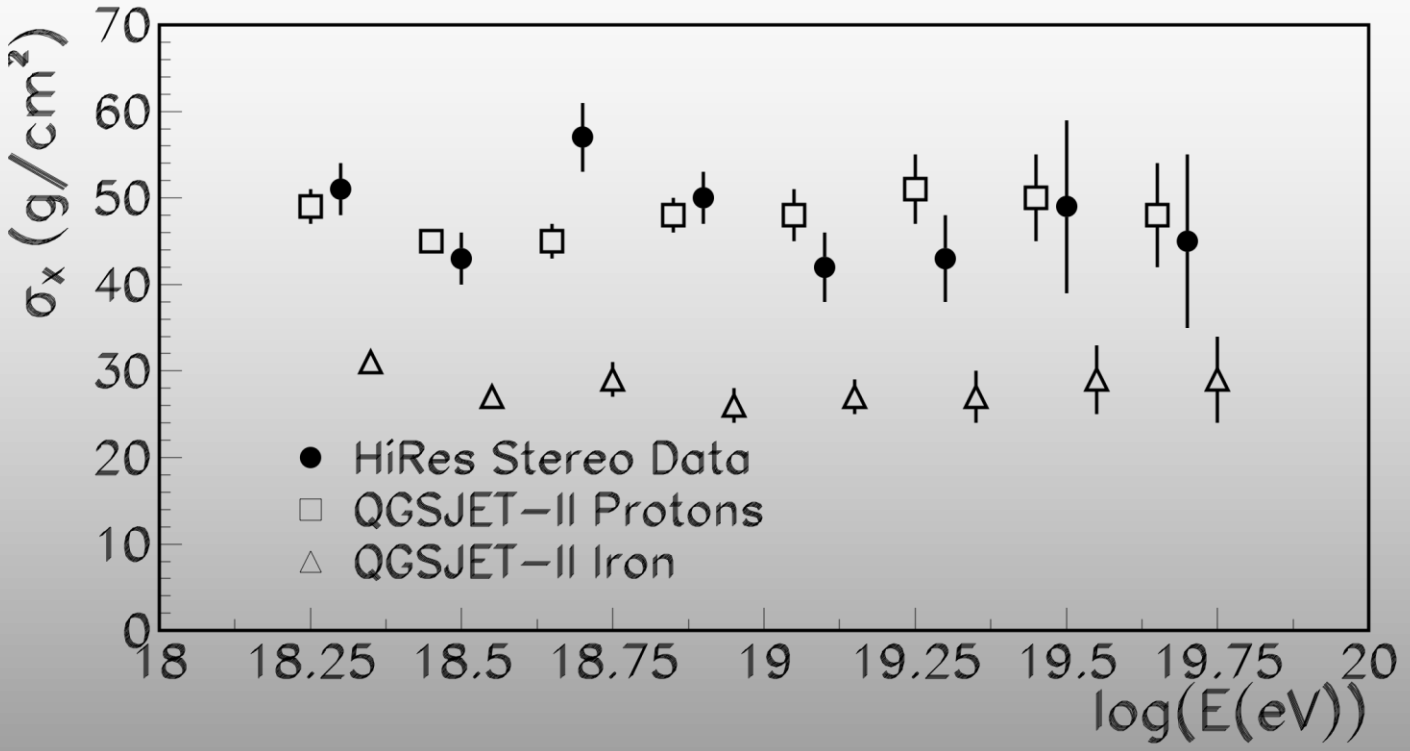

Comparison of Xmax fluctuations with predictions for Proton and Iron using QGSJET-II. Truncated Gaussian fit.

Elongation rate corrected for detector acceptance and comparison with previous HiRes results and PAO

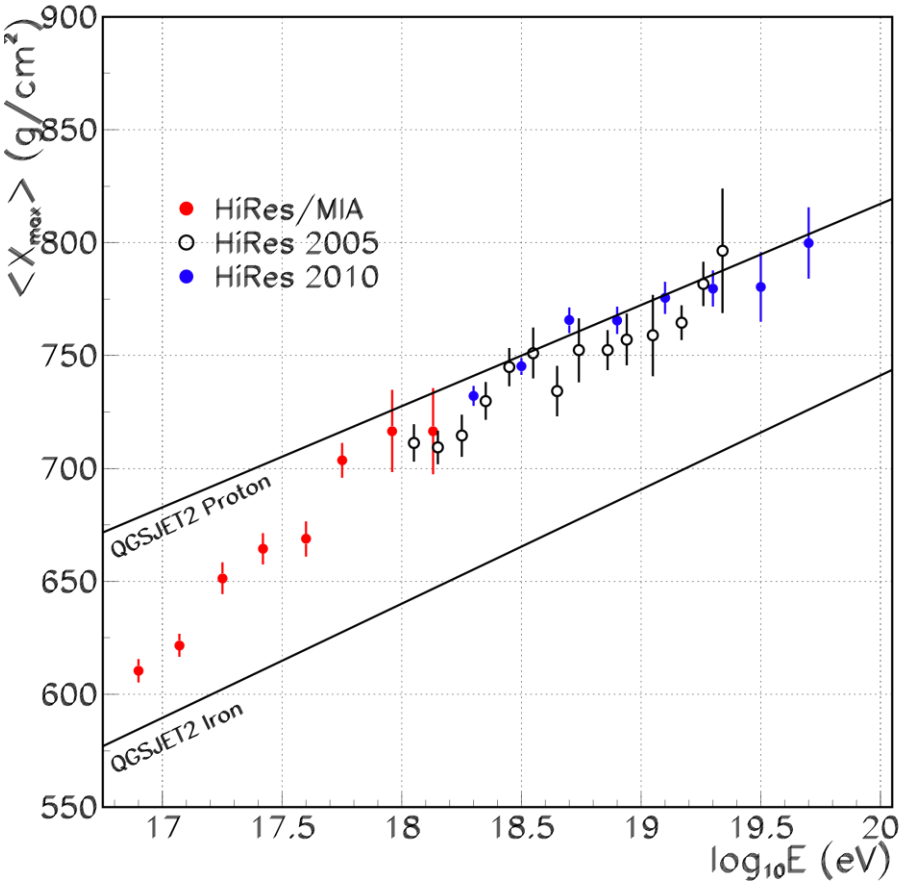

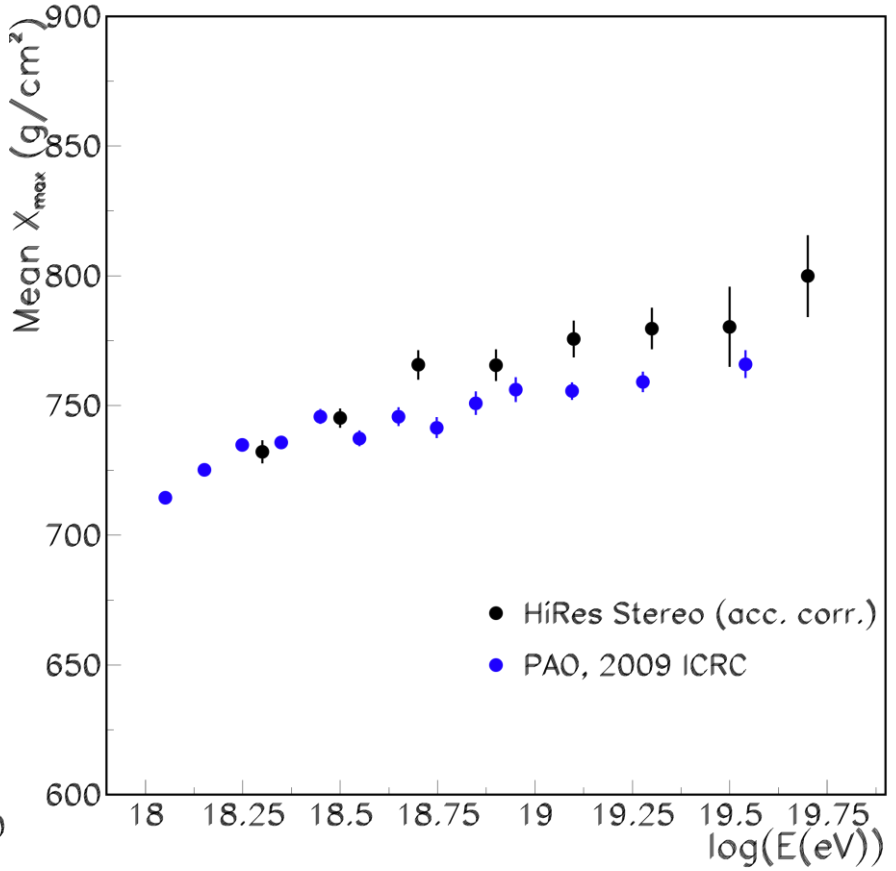

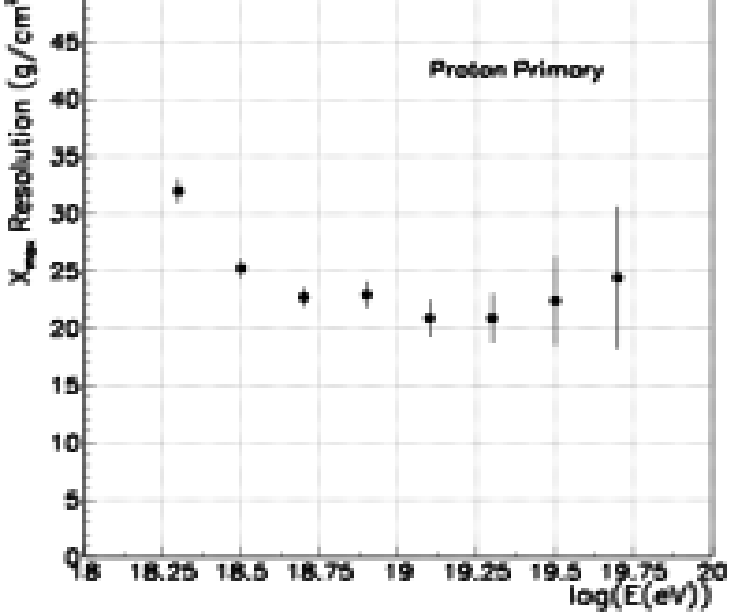
Proton Primary
log(E(eV))

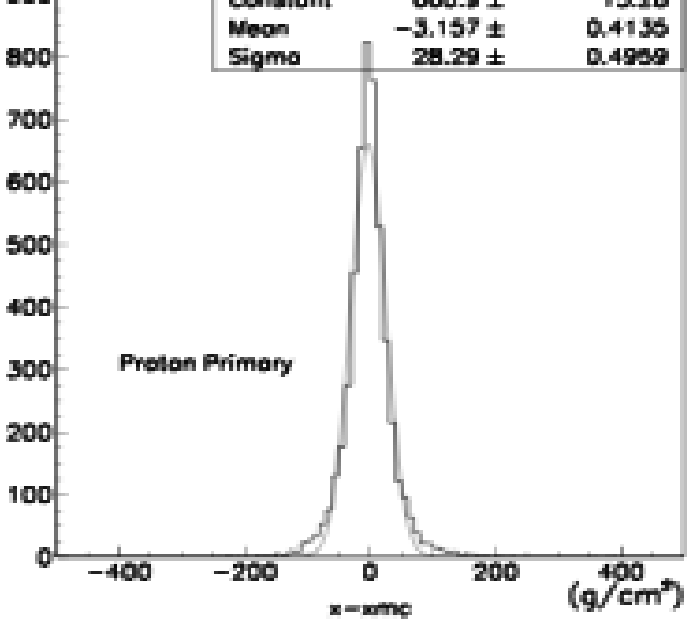
Mean −3.157 ± 0.4135
Sigma 28.29 ± 0.4959
Proton Primary
x−xmc
(g/cm²)

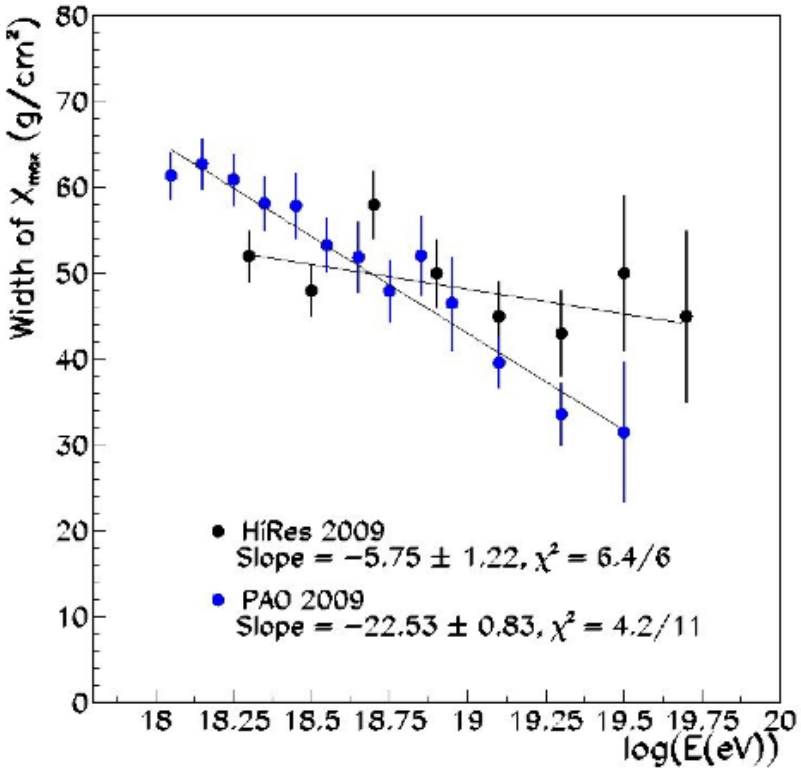
Width of X_{max} (g/cm²)
HiRes 2009
Slope = −5.75 ± 1.22, χ² = 6.4/6
PAO 2009
Slope = −22.53 ± 0.83, χ² = 4.2/11
log(E(eV))

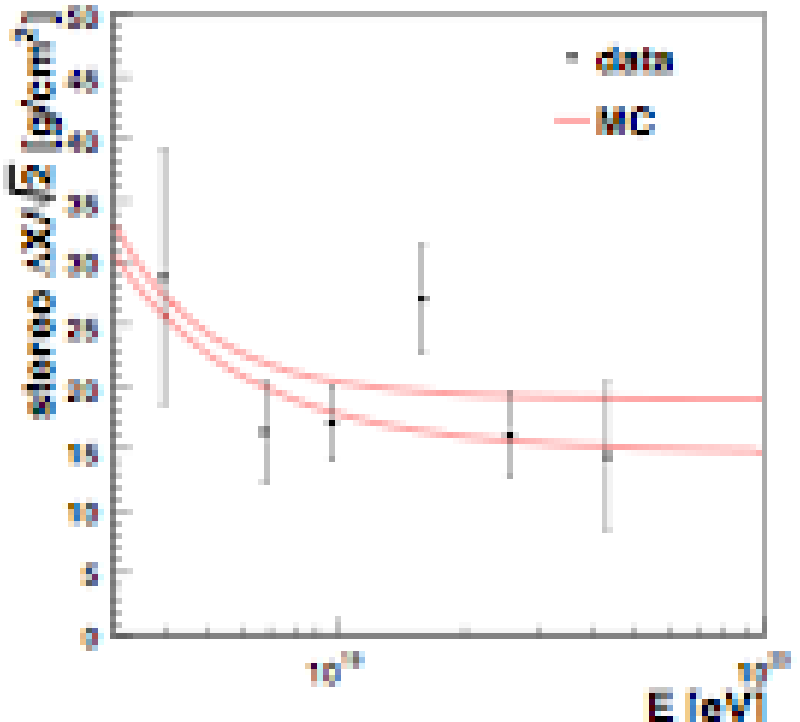
data
MC
E [eV]

y 2009

Conclusions_01

- A cut off has now been clearly observed by the HiRes mono and stereo data in the Northern hemisphere cosmic ray flux at the 5 sigma level.
- An ankle structure is clearly seen in HiRes and in monocular TA data.
- The composition is consistent with a light, mostly protonic flux.
- The cut-off is consistent with the GZK prediction

Anisotropy

- No significant large scale anisotropies found by HiRes at any energy.
- AGASA claim of clustering is not supported by HiRes data
- However, one AGASA triplet becomes a quartet - significance still not strong.
- Search for correlations with BL-Lacs – low statistical signifiance effect published, confirmation required – not seen by PAO
- No evidence for correlations with AGN's applying PAO cuts.
- No evidence for correlations with LSS

HiRes AGN Correlation Study

Take-home message:

- Apply PAO cuts - no significant correlation
- Split data in half and search for most significant cuts in z, theta, and Emin
- Apply cuts to second half of data - no significant correlation
- Use total data set using method proposed by Finley and Westerhoff (penalty for scanning over entire data set taken into account) - no significant correlation

HiRes with PAO cuts

- PAO has maximum significance for < 3.1 deg., Emin=.56 EeV, Zmax=.018
- 8 pairings from 13 events in confirming set.
- Expect 2.7 chance pairings
- PAO chance prob. = 0.0017
- HiRes with PAO cuts (10% shift)
- 2 pairings from 13 events
- Expect 3.2 chance pairings
- HiRes chace prob. = .82

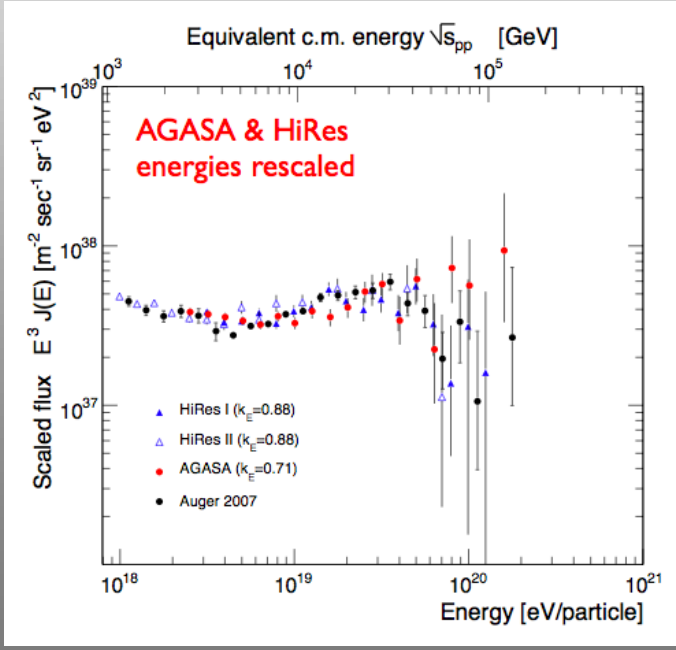

Pao spectrum, 10% energy shift

Independent HiRes search

- First data set scan
- Strongest correlation 1.7 deg., 15.8 EeV, zmax =0.02. (chance prob = 0.005)
- Apply to second data set
- 14 correlations out of 101 events
- Chance probability .15

HiRes correlation with Veron AGN catalogue in North

Black - AGN's

Blue - HiRes data

Red - correlated events (from scan in z, theta and Emin)

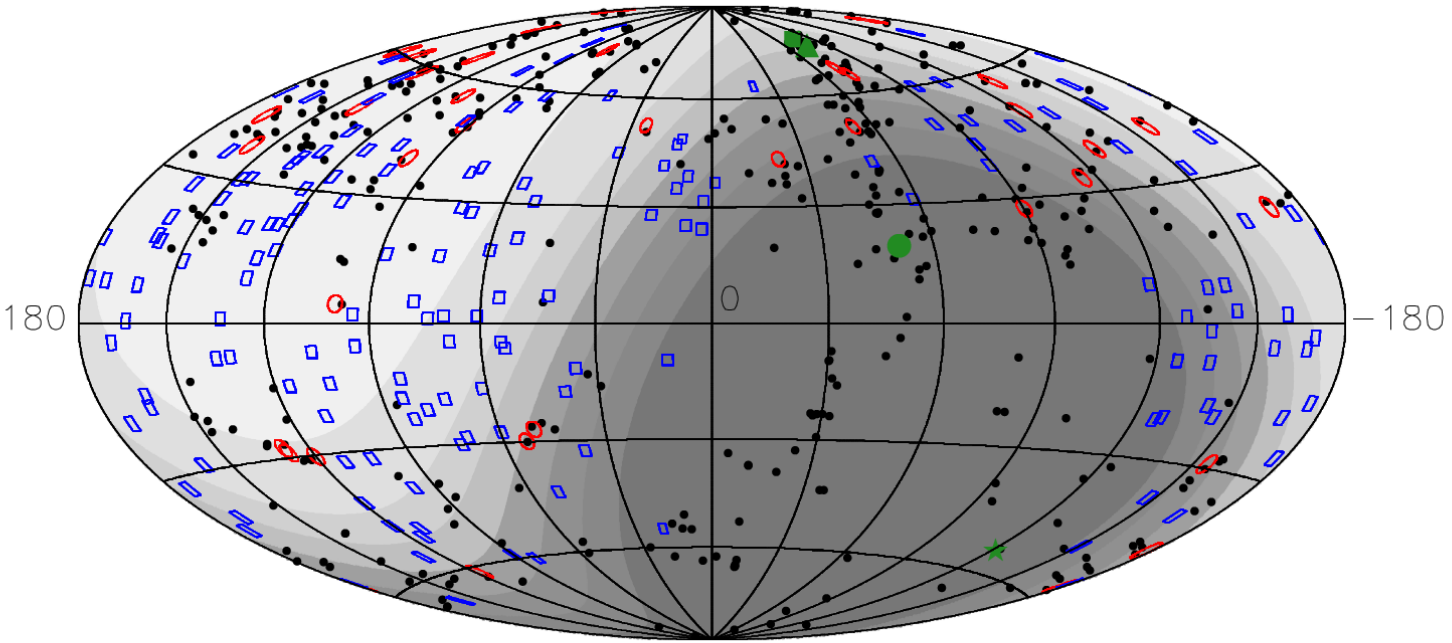

Search for correlations with LSS

- Assume UHECR source distribution follows density distribution of matter (LSS)
- Assume magnetic effects can be described by a Gaussian smearing angle
- Look for significance of correlation as a function of smearing angle and energy.

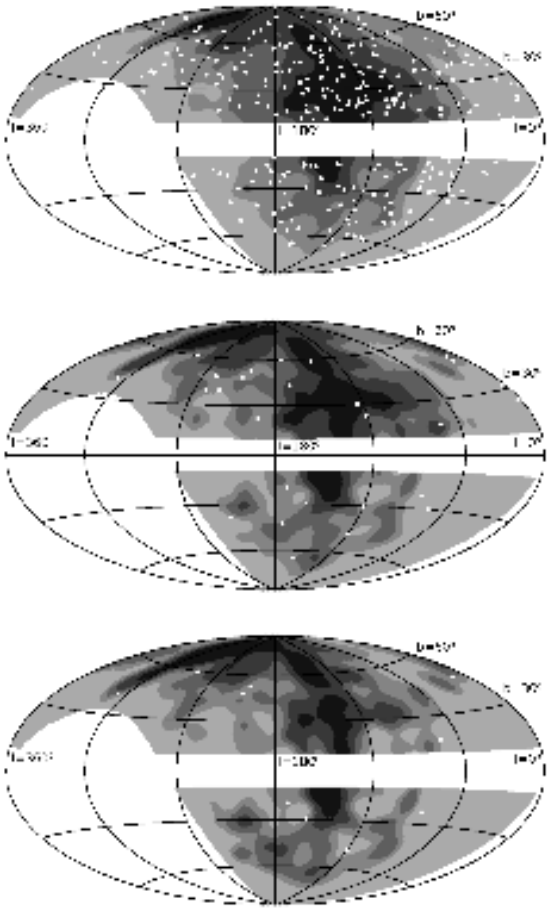

Fig. 2.— Hammer projection (galactic coordinates) of $\widetilde{\Phi}$ (flux times exposure) with threshold energies 10 EeV (top panel), 40 EeV (middle), and 57 EeV (bottom). Darker gray indicates a higher value; the bands are chosen such that each band contains 1/5 of the total flux (weighted with exposure). Excluded regions, viz. the galactic plane ($|b| < 10°$) and the region outside the HiRes field of view, are shown in white. White dots indicate HiRes events. All maps are produced with $\theta_s = 6°$.

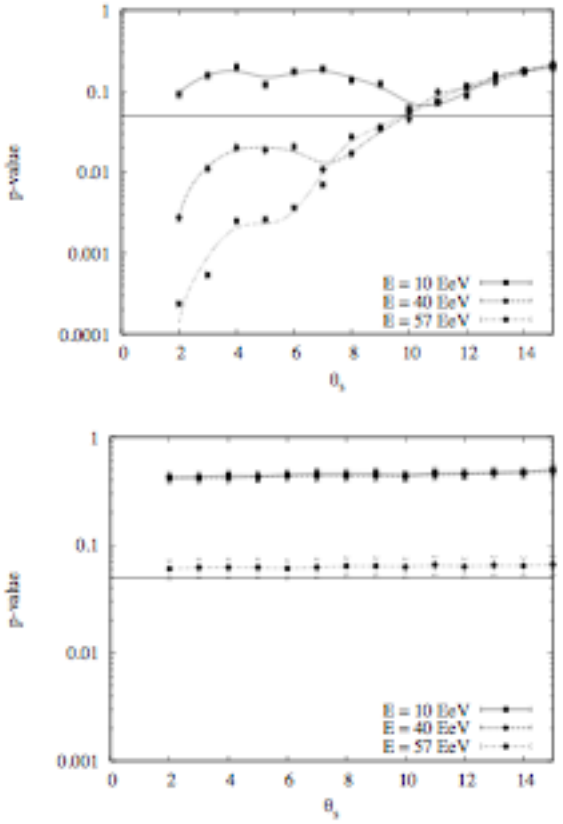

(a) For the threshold energies of 40 EeV and 57 EeV, the tests show disagreement between data and the matter tracer model for $\theta_s \leq 10°$. Within this parameter range, a source distribution tracing the distribution of matter is excluded at a 95% confidence level.

(b) For the threshold energy of 10 EeV, the test shows agreement between data and the matter tracer model.

Results

- Choose 95% c.l. exclusion to quote, a priori.
- For isotropic model, get good agreement.
- **For local LSS model get poor agreement.**
- Exclude correlation at 95% c.l. for $\theta_s < 10°$, $E \geq 40$ EeV
- At 57 EeV, Auger point, exclude correlation at 5° at **99.5%** c.l.

Conclusion_02

- No evidence of correlations with AGN's in Northern Sky
- No evidence of correlation with local LSS with smearing angles less than 10 degrees in Northern Sky

HiRes is complete. New data now becoming available from TA experiment

Systematic issues with Xmax fluctuations

- Control of Xmax resolution
- Undersampling
- Acceptance bias

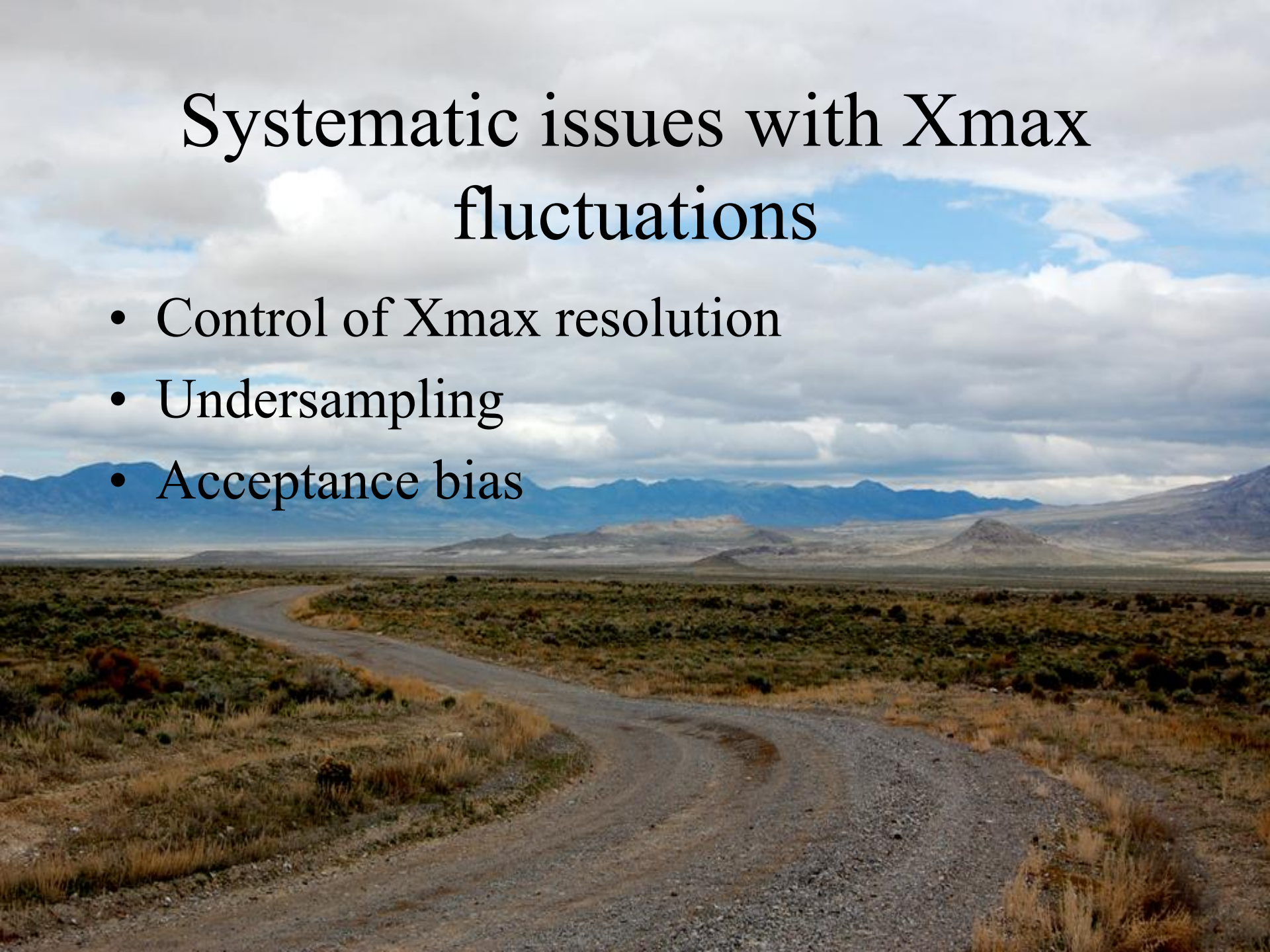

Control of Xmax Resolution

- Monte Carlo Simulation
- Stereo Xmax comparison – agrees with MC predictions
- While stereo runs out of statistics at the highest energies, HE events lie in the same Rp, zenith angle domain as higher statistics lower energy events. No geometrical or signal strength difference of significance
- Atmospheric effects. Cut on “better than average” and “worse than average” atmosphere data. No difference.

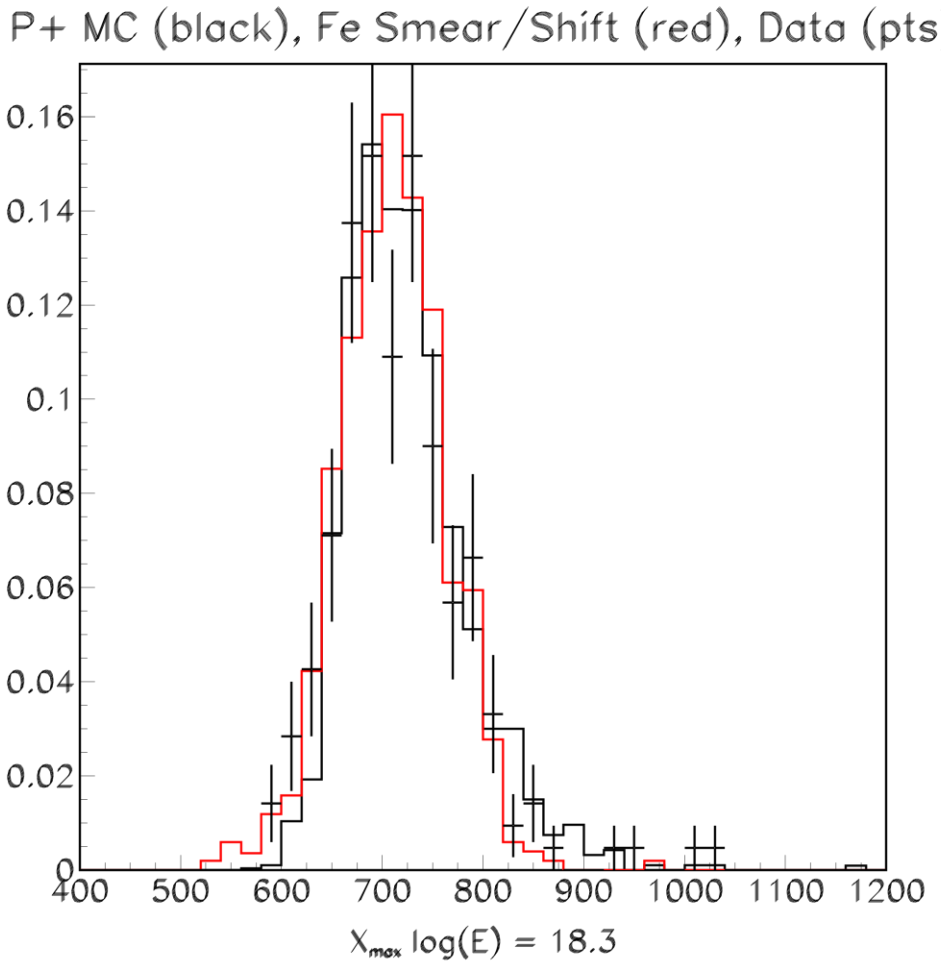

Effect of taking simulated Fe events, smearing by an ADDITIONAL 40 gm/cm2 Resolution (65gm/cm2 in total) and shifting peak to coincide with proton dist

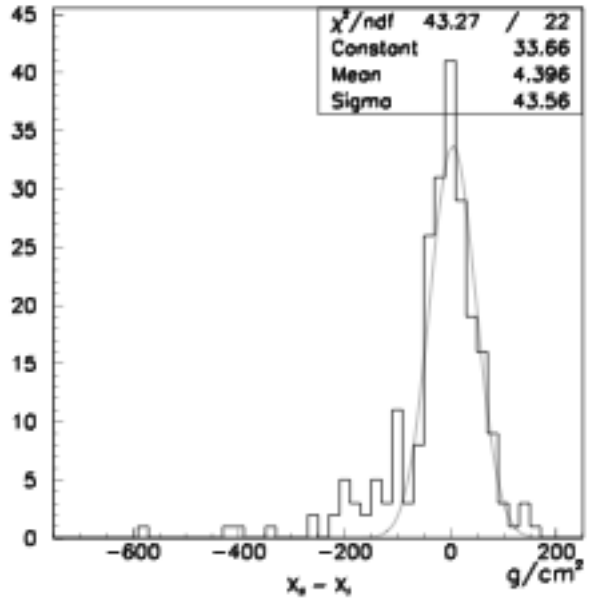

Incompatible with measured XmaxI-XmaxII distribution.

Undersampling

- Problem if width of distribution is smaller than "parent distribution" – undersampling cannot broaden a distribution.
- RMS's of ~25 gm/cm2 have a ~ 10% chance of occuring for N~20

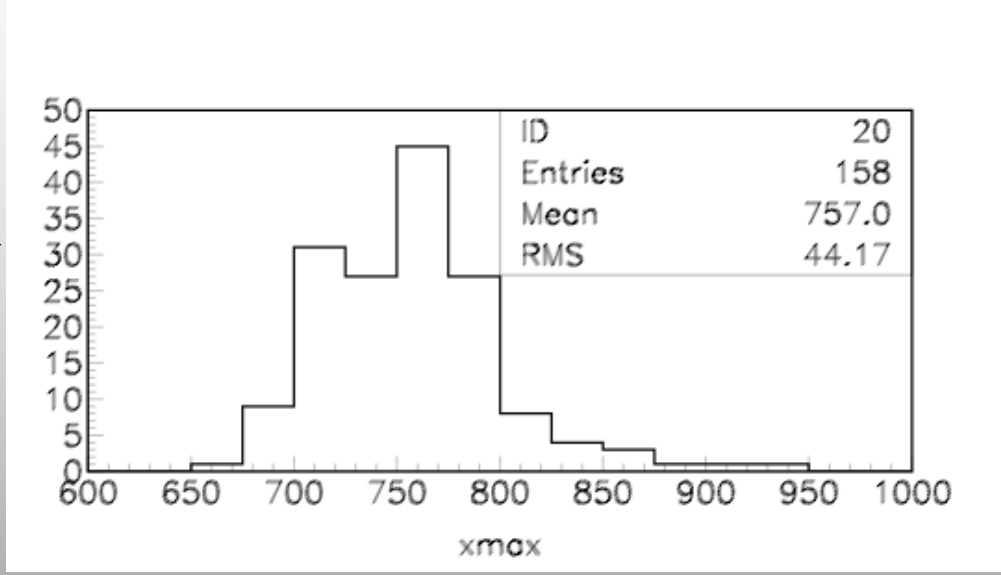

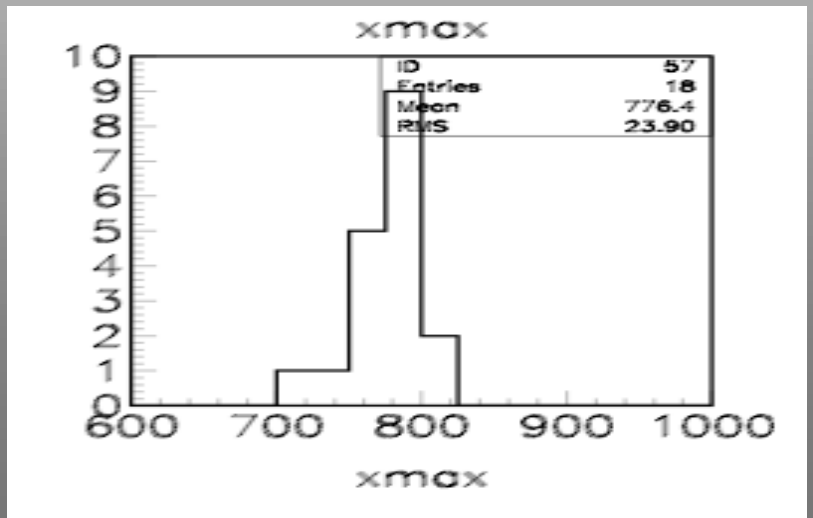

Acceptance bias

- Xmax distributions can be distorted by cuts or variation in detector acceptance.
- Difficult to produce a broadening of Xmax distribution with energy.
- Simulations indicate that HiRes acceptance improves with energy. Cuts remove any residual energy dependence.

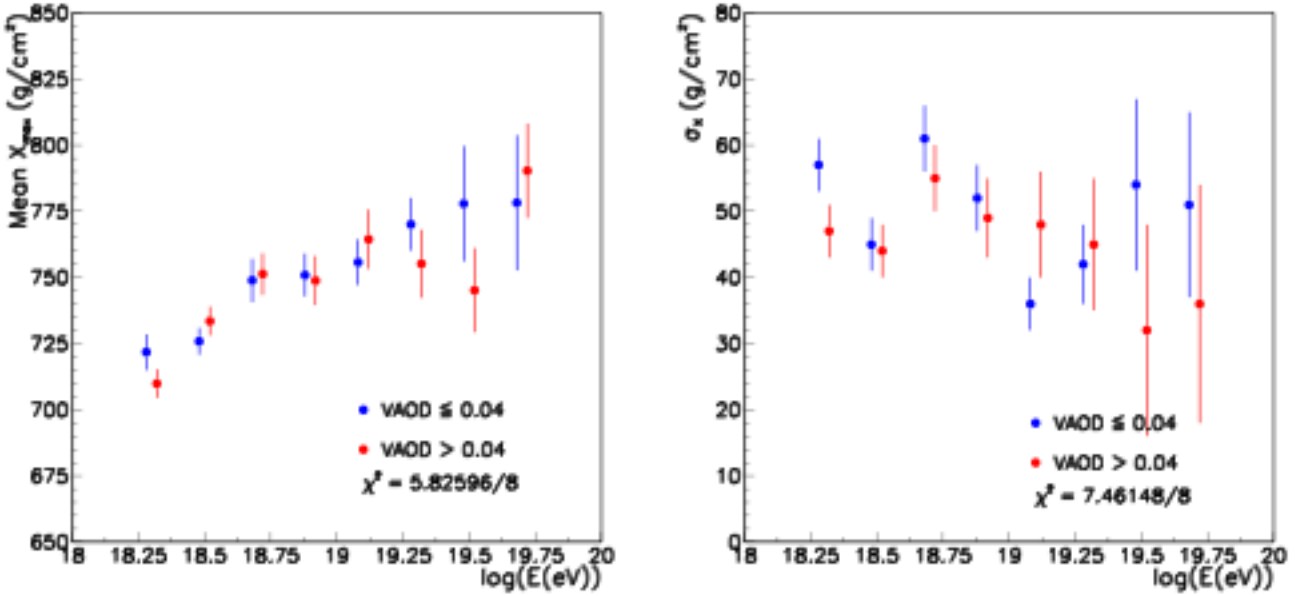

Figure 2: *Left:* Observed $<X_{max}>$ of HiRes stereo data for two independent samples, with VAOD less than (blue) and greater than (red) the mean value of 0.04. The elongation rates for these samples are (48.4 ± 3.8) g/cm^2/decade and (47.2 ± 2.5) g/cm^2/decade respectively. *Right:* Widths of X_{max} distribution in HiRes stereo data for two independent samples, with VAOD less than (blue) and greater than (red) the mean value of 0.04. A fit of these data to constant width yields (48.6 ± 1.8) g/cm^2 and (47.4 ± 2.1) g/cm^2 respectively. Note that in both plots a small horizontal offset has been applied to visually separate the points.

Simulated proton and data biases

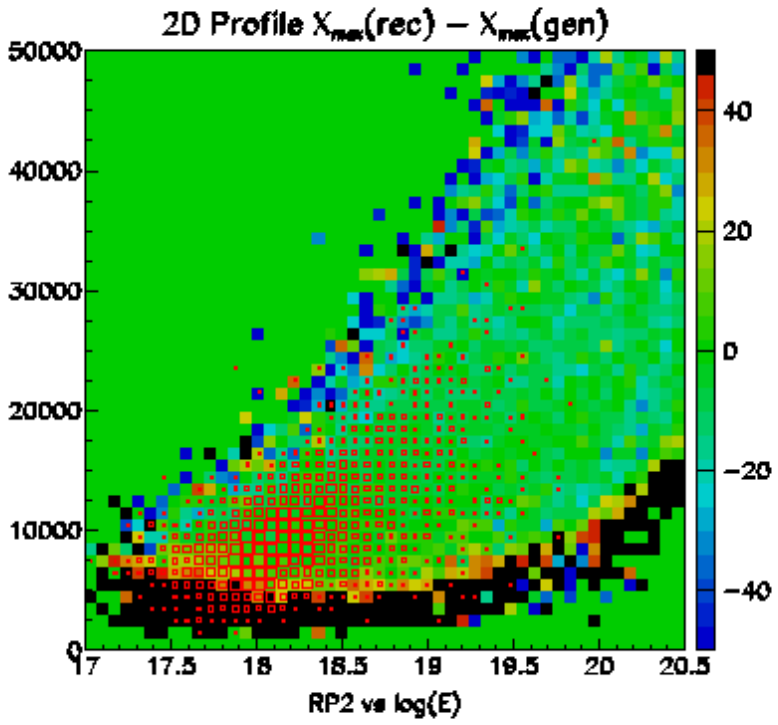

Figure 9: Same as previous plot, with HiRes stereo data (passing all cuts except those on energy and RP_2) superimposed as a red box plot.

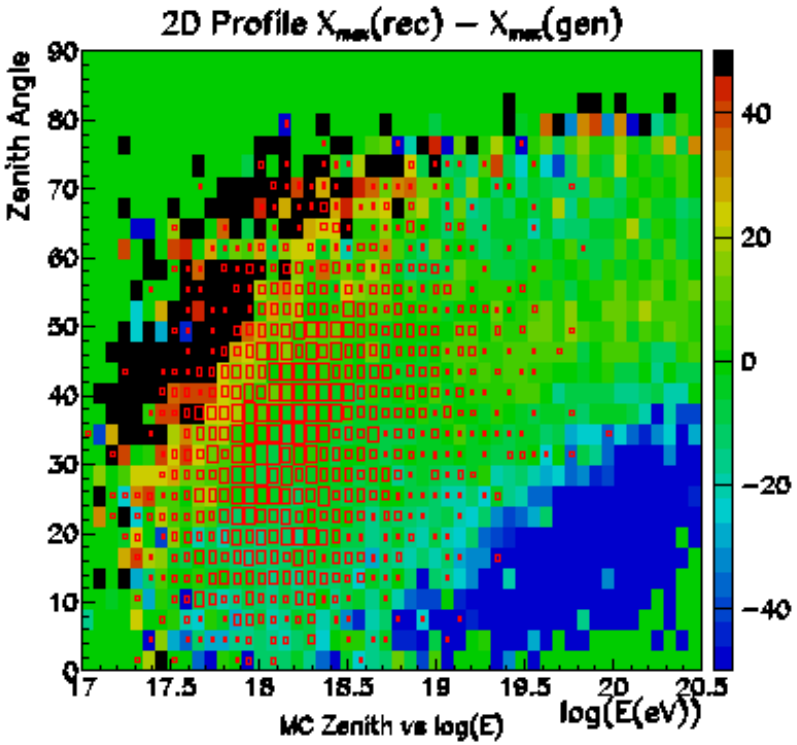

Figure 13: Same as previous plot, with HiRes stereo data (passing all cuts except those on energy and zenith angle) superimposed as a red box plot.

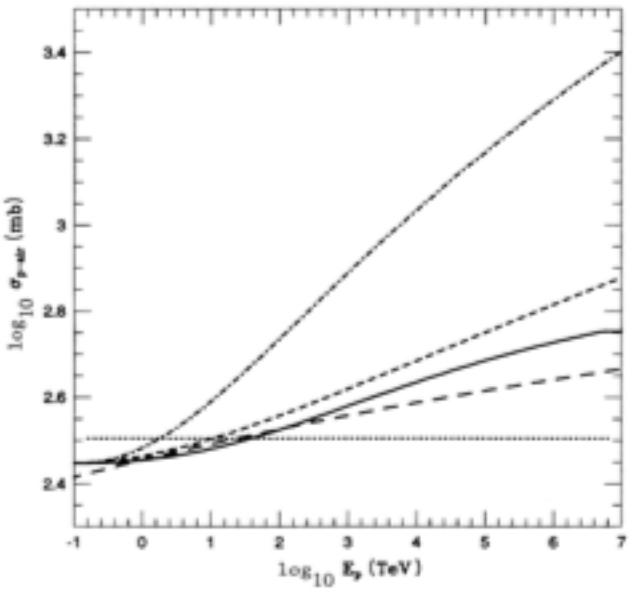

FIG. 9. Energy dependence of different cross-section models. The solid line shows the cross section used in the composition calculation; dots—constant cross section; long dashes—$\ln(s)$ energy dependence; short dashes—$\ln^2(s)$ energy dependence; dash-dots—LM model.

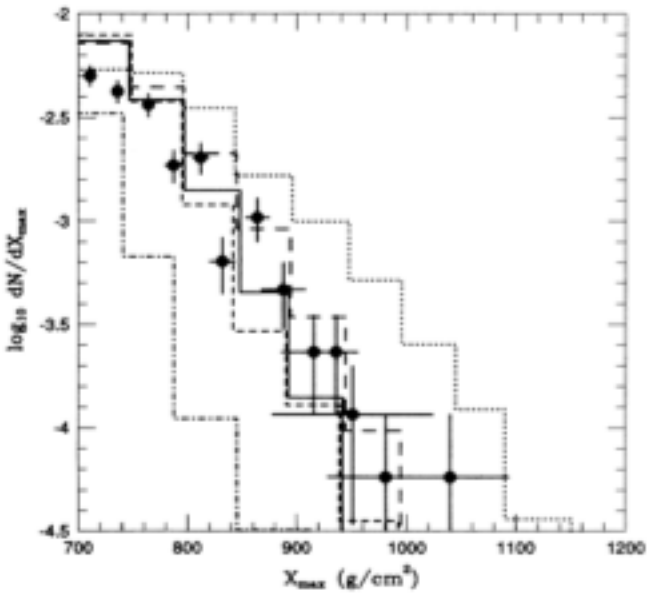

FIG. 10. X_{max} distributions for simulated proton showers with different proton-air inelastic cross sections compared to the tail of the experimental distribution. All showers are with energy above 1 EeV. The cross sections are coded as in Fig. 9.

Illustration of effect of changing total inelastic cross-section (keeping everything else constant in minijet model T.K. Gaisser et al., Phys. Rev D 47, 1993, p.1919)

Comparison of predicted elongation rates using different Xmax definitions

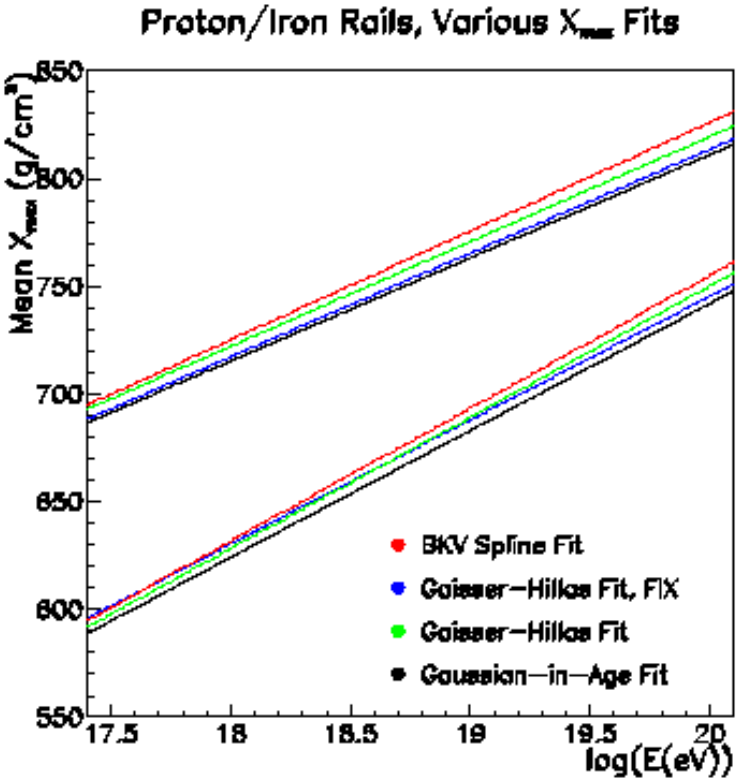

Figure 2: Evolution of the mean X_{max} for a set of CORSIKA [4] (QGSJET01 high-energy hadronic model) simulated proton (upper rail) and iron (lower rail) showers, under four different X_{max} definitions. Red – "spline" fit to extract peak of longitudinal distribution. Blue – fit to Gaisser-Hillas function [5] with X_0 and Λ fixed. Green – Gaisser-Hillas fit, all parameters floating. Black – Gaussian-in-age fit.

Upper limit on HiRes –II Xmax Resolution

- If HRI and HRII were identical detectors, Delta(Xmax) = 45 gm/cm2 implies each detector has resolution of 45/sqrt(2) = 30 gm/cm2
- HRI has ~ 1.5 x worse resolution (limited FOV), so Delta(Xmax) = 45 gm/cm2 implies a HRII resolution of ~25gm/cm2, in agreement with MC calculations

Systematic errors in <Xmax>

- 15 +/- 1.8 gm/cm2 shift (to lower values) of MC data due to energy-independent acceptance bias
- 3.3 gm/cm2 uncertainty in Data due to alignment and survey errors
- 0.7 gm/cm2 uncertainty due to MC statistics.

Comparison of data and p-QGSJET02,01 fluctuation widths
Use 2-sigma truncated gaussian width to fit Xmax distr.
Detector resolution is NOT deconvoluted!

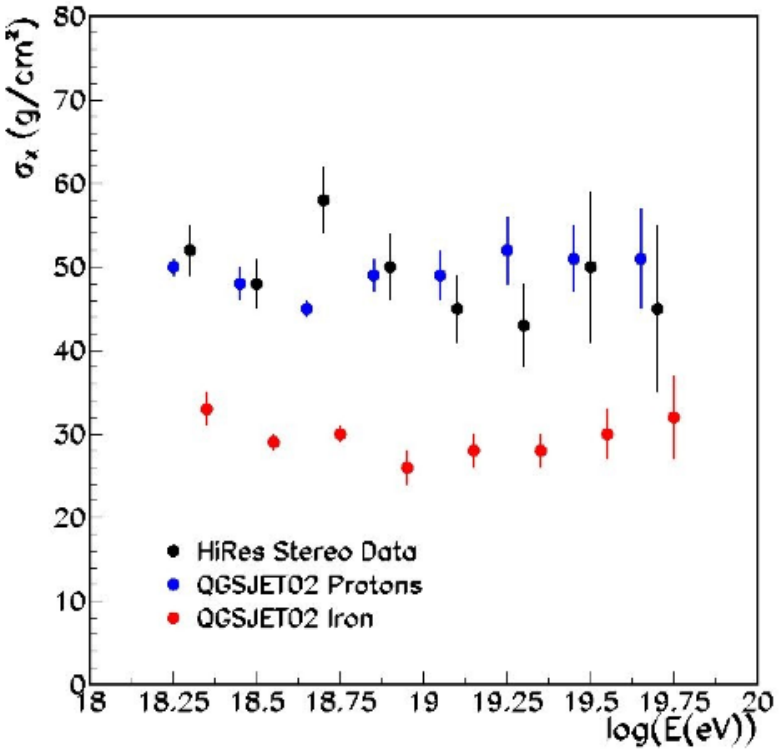

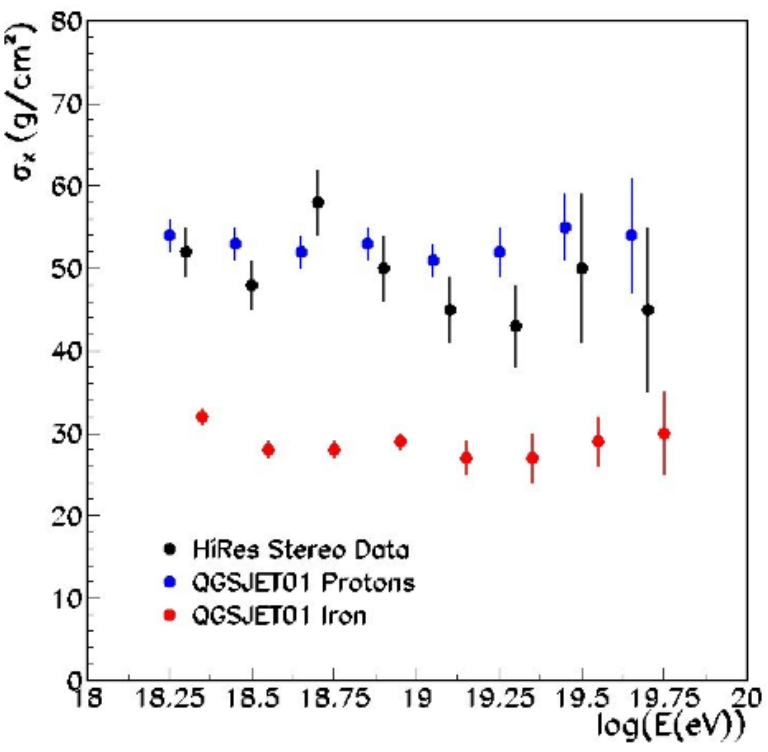

Data/MC Comparison - Stereo

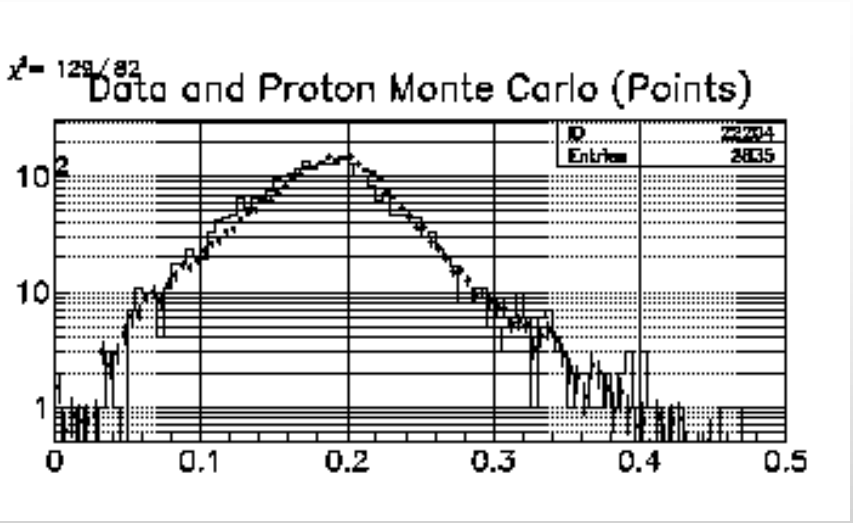

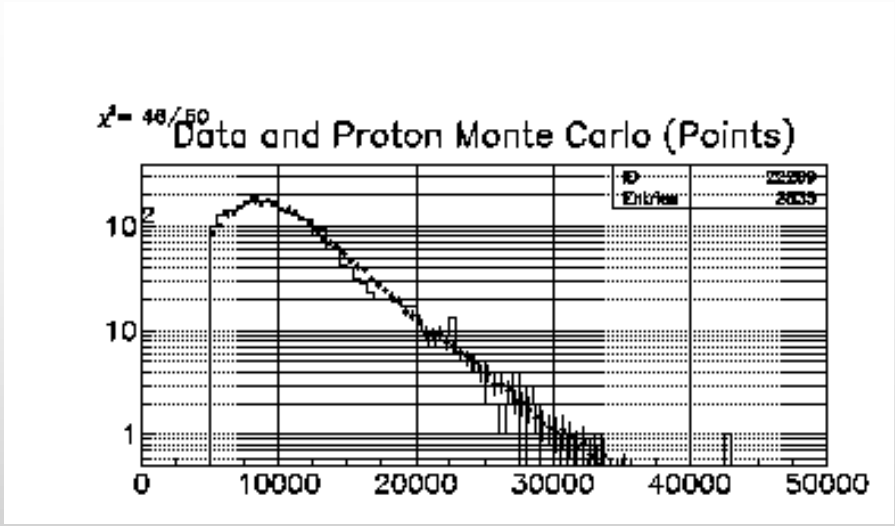

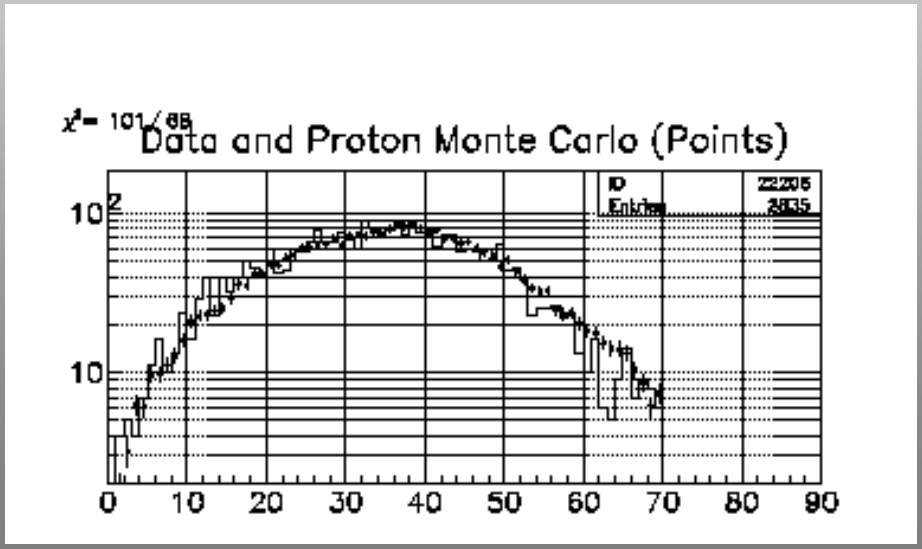

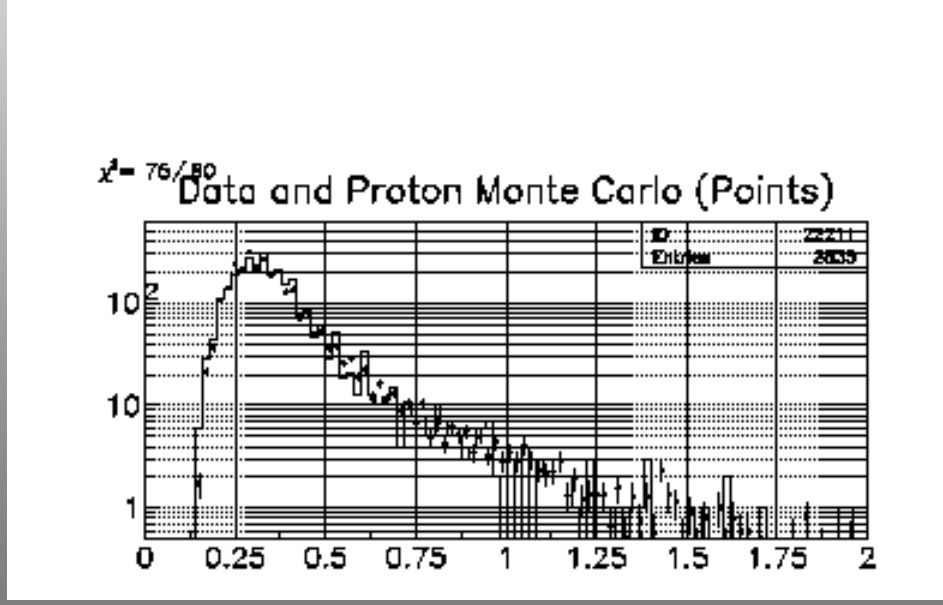

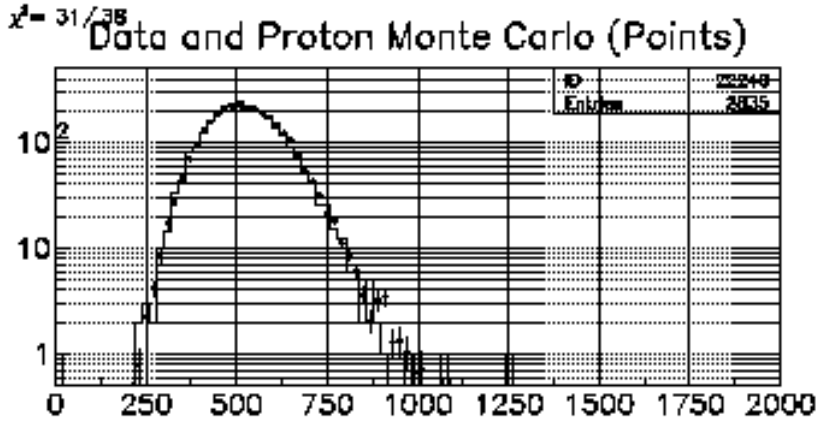

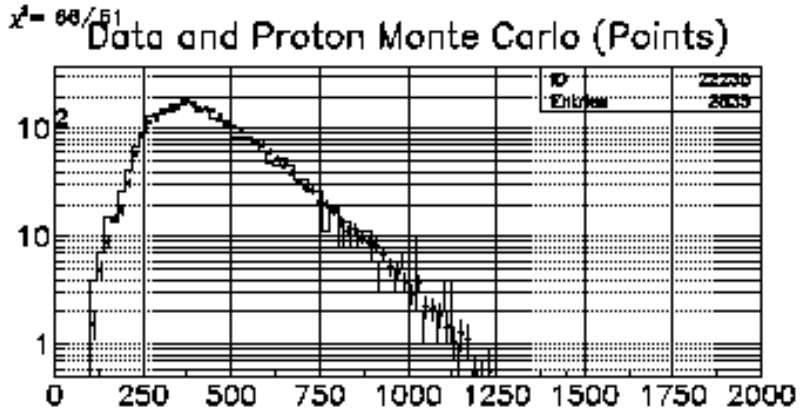

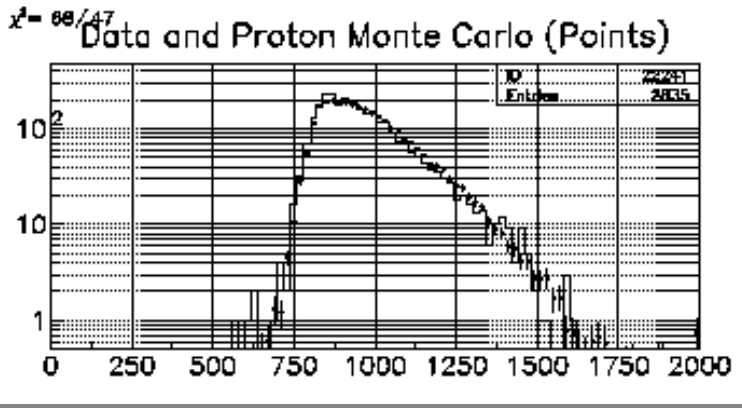

Excellent agreement between Simulation and observables

Data and MC Cuts to minimize reconstruction error and bias

- Good weather cuts
- Zenith angle < 70 deg.
- Zenith angle error < 2 deg.
- Xmax uncertainty < 40 gm/cm2
- Rp with respect to HiRes-2 > 10 km.
- Xmax bracketed in HiRes-2 FOV
- Energy > l0^18.2 eV.
- 815 events survive these cuts.